# Supplementary information

## ESI 1a: Additional information on bulk characterisation

*Table S1 Rietveld refinements of the XRD patterns collected with the laboratory source (Cu K$\alpha$ = 1.5406 Å) – the confidence of the fits and the lattice parameters for these fits are presented. Isotropic atomic displacements and isotropic lattice strains were used in the Rietveld refinement. The occupancy of Mn and Co in the 3a Wyckoff site are assumed to be invariant at 10 % whilst Ni is allowed to iterate (with at most 80 %). The remaining occupancy is filled by Li and these amounts are substituted by Ni in the Li occupancy for the 3b Wyckoff site – this is the Li/Ni anti-site mixing.*

| **NMC811** | ***a* / Å** | ***c* / Å** | ***Lattice strain / %*** | **$R_{wp}$ / %** |
|---|---|---|---|---|
| **ALD NMC811** | 2.8714(0) | 14.204(8) | 2.(3) | 2.11 |
| **NMC811** | 2.8716(3) | 14.205(6) | 1.(4) | 1.93 |

| | **Site** | **Atom** | **x** | **y** | **z** | **Occupancy** |
|---|---|---|---|---|---|---|
| **ALD NMC811** | *3a* | Ni | 0 | 0 | 0 | 0.787(6) |
| | | Mn | 0 | 0 | 0 | 0.1 |
| | | Co | 0 | 0 | 0 | 0.1 |
| | | Li | 0 | 0 | 0 | 0.012(4) |
| | *3b* | Li | 0 | 0 | 0.5 | 0.987(6) |
| | | Ni | 0 | 0 | 0.5 | 0.012(4) |
| | *6c* | O | 0 | 0 | 0.2566(7) | 1 |
| **NMC811** | *3a* | Ni | 0 | 0 | 0 | 0.781(2) |
| | | Mn | 0 | 0 | 0 | 0.1 |
| | | Co | 0 | 0 | 0 | 0.1 |
| | | Li | 0 | 0 | 0 | 0.018(8) |
| | *3b* | Li | 0 | 0 | 0.5 | 0.981(2) |
| | | Ni | 0 | 0 | 0.5 | 0.018(8) |
| | *6c* | O | 0 | 0 | 0.2554(8) | 1 |

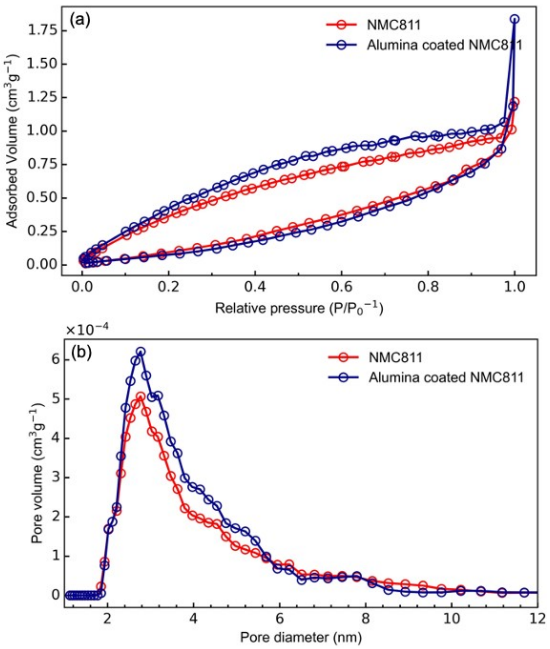


*Figure S0: (a) $N_2$ adsorption-desorption isotherm and (b) Pore size distribution analysis for NMC811 and ALD alumina coated NMC811 powder samples.*

# ESI 2: Fabrication of coin cells

## Electrode casting

Electrodes for cycling in coin cells were fabricated by a conventional electrode casting procedure. A mixture of *N*-Methyl-2-pyrrolidone (NMP, Sigma-Aldrich, 99.5 %, anhydrous), Kynar HSV900 polyvinylidene difluoride (PVDF, Arkema), NMC811 and Super P carbon were homogenised using a THINKY planetary mixer (Intertronics, SR-500) for 10 min at 2000 rpm. The slurry had NMC:Carbon:PVDF in a 90:5:5 mass ratio. This slurry was coated onto aluminium current collector foil (MTI corporation, 15 µm thickness) with a doctor blade (235 $\mu m$ gap). The casted electrode film was dried under a flowing nitrogen atmosphere at 75 °C for up to 40 min until visibly dry. Subsequently 14 mm discs (~6.8 mg cm$^{-1}$) were cut and dried again at 120 °C in Büchi ovens under vacuum for 12 h before airless transfer into an Ar GB.

## Coin cell preparation

$LiFePO_4$ electrodes (LFP, MTI Corporation) were chosen as the counter electrode against NMC811 to avoid the solvent degradation products produced at the positive electrode (NMC811) being reduced at either Li or graphite negative electrodes as the LFP voltage plateau sits at 3.54 $V_{Li}$. LFP electrodes were cut into 15 mm discs (dried at 120 °C under vacuum for 12 h) to achieve a 1.1-1.2 ratio in the capacity of the negative:positive (N:P) electrode, to ensure only the voltage plateau of $LiFePO_4$ is swept.

*LFP*|Li cells were assembled in CR2032 stainless steel coin cells (Cambridge Energy Solutions, 316 grade) using a 17 mm polypropylene separator (Celgard 3501; 25 µm) wetted

with 65 µL of 1 M $LiPF_6$ in EC/EMC. After cycling, these cells were disassembled inside the glovebox and the delithiated $LiFePO_4$ electrode was rinsed with DMC. Once the solvent was evaporated, it was ready for use as a counter electrode.

*NMC811*|delithiated-LFP cells were also assembled with a combination of polypropylene separator (in direct contact with the positive electrode to prevent delamination of the NMC811 onto the glass fibre) and a glass fibre one (not in direct contact with positive electrode). Glass fibre retains more electrolyte volume than the Celgard separator, allowing enough electrolyte to be obtained for *ex-situ* post-mortem analysis. Sets of cells were assembled to assess the influence of the $Al_2O_3$ coating on the 1 M $LiPF_6$ in EC:EMC (3:7 (v/v)) electrolyte. Each set of cells had one cell containing the baseline uncoated NMC811, the rest comprising ALD NMC811. 120 µL of electrolyte was used to maintain good wetting of the dual separators.

Graphite electrodes (Argonne National Laboratory CAMP facility) were cut into 15 mm discs for a N:P ratio of 1.1-1.2 for cell balancing against casted NMC811 electrodes (14 mm). Electrodes were all dried at 120 $^oC$ under vacuum for 12 h before airless transfer into the Ar glovebox for assembly. *NMC811*|graphite cells were subsequently assembled in a similar manner to the *NMC811*|delithiated-LFP cells with a double separator format and 120 $\mu L$ of 1 M $LiPF_6$ in EC:EMC (3:7 (v/v)) with 2 wt% VC. After the long-term cycling, these cells were disassembled within the Ar-glovebox and the aged NMC811 electrodes rinsed with DMC before drying *in-vacuo.*

*NMC811*|Li coin cells analogous to the *LFP*|Li were assembled for the X-ray absorption spectroscopy (XAS) measurements of the surface chemical states of the (un)coated NMC811. All cells were disassembled in the Ar GB and electrodes were rinsed with DMC before drying *in-vacuo*. All samples were transferred to the XAS sample chamber *via* an air-less transfer unit.

## ESI 3: Details about NMR parameters

$^{27}Al$ is a quadrupolar nucleus (quadrupolar spins > 1/2, $^{27}Al$ spin $I$ = 5/2) with 100 % natural abundance and has ~20 % receptivity of that of $^{1}H$ indicating it is a readily observed nucleus for common NMR setups. $^{27}Al$ isotropic chemical shifts provide useful chemical information about the neighbouring nuclei with oxides spanning from approximately 80 – 0 ppm [1–3] whilst (oxy)fluorides span 59 – -17 ppm. depending on the degree of fluorination. These chemical shifts are also influenced by the number of coordinating nuclei: tetrahedrally coordinated Al is the most deshielded (~80 ppm, γ-$LiAlO_2$3–5) and Al in octahedral configurations are the most shielded (*e.g.*, 5 ppm in α-$Al_2O_3$).[2] Penta-coordinated Al can also be detected in $^{27}Al$ NMR spectroscopy with intermediate shifts around the 20 – 52 ppm range and more importantly, are an indicator of disordered or amorphous alumina phases.[6–10] If doping of Al from the

coating into the layered metal oxide host structure occurs, resulting in a local paramagnetic environment for the Al, the Fermi-contact interaction between $^{27}$Al and the unpaired electrons of Ni (or Mn) results in dramatically lower ppm values (< -1300 ppm for Ni-rich cathodes).[11,12] The quadrupolar interaction between the quadrupole moment of the nucleus and the local electric field gradient is described with the quadrupolar coupling constant, $C_Q$ and is highly dependent on the local environment.

To be quantitative when measuring NMR, all environments should be excited to the same degree. A range of possible $C_Q$ from the different Al environments mean that each type of Al site will have its own excitation profiles. Therefore, a flip angle smaller than $\frac{\pi}{2}$ is used to linearly excite all the different Al environments. Due to the scarcity of the Al (ICP-MS an Al concentration of 223 ppm w/w), a $\frac{\pi}{3}$ flip angle was chosen to compromise between the signal-to-noise obtained and quantitative NMR. Appropriate recycle delays are also required but a longitudinal relaxation ($T_1$) measurements were not practically feasible, 220k scans with a 500 ms recycle delay requiring over 31 h of acquisition time. Double frequency sweep (DFS) enhanced (20 kHz rf field strength DFS sweep from 1.25 MHz – 225 kHz over 2600 $\mu s$) Hahn-echo experiments (16.4 T, 1.3 mm DR probe and 50 kHz MAS spinning speed) were used to acquire signal in reasonable times for the comparisons.

Three recycle delays (75, 225 and 500 ms) were tested on the as-synthesised ALD NMC811 material, taking into consideration the faster spin-lattice relaxation arising from $^{27}$Al being quadrupolar, and the heteronuclear and electron-nuclear dipolar interactions that diamagnetic $^{27}$Al should experience due to nearby $Ni^{3+/4+}$ and $Mn^{3+/4+}$ in the NMC811.

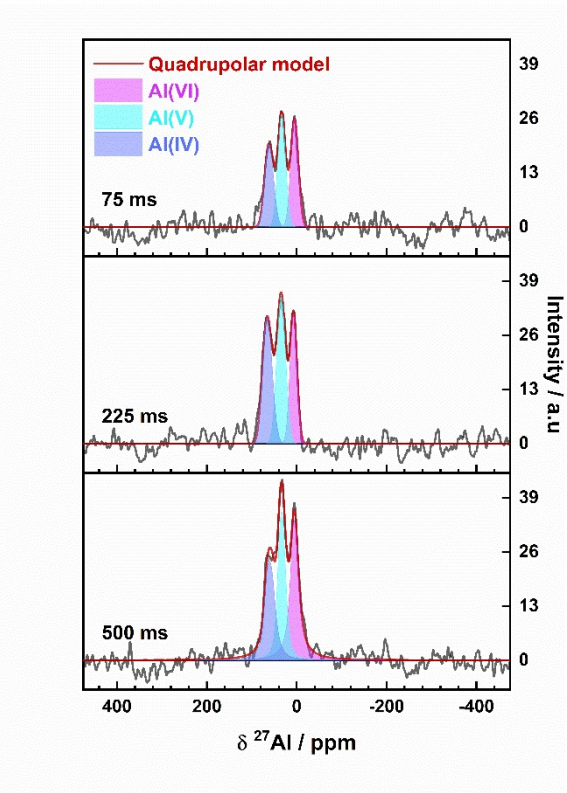


*Figure S1: $^{27}$Al double frequency sweep (DFS) enhanced Hahn-echo spectra of the pristine ALD NMC811 sample recorded with a recycle delay of 75, 225 and 500 ms – each spectra is acquired with the same number of scans with the same sample mass. Recorded at 16.4 T with a spinning frequency of 50 kHz; the DFS was swept between 1 MHz – 225 kHz about the receiver frequency (at 40 ppm) with a rf pulse power of 20 kHz over 2.5 ms whilst the echo was obtained using a soft rf pulse of 8 kHz and a $\frac{\pi}{6}$ flip angle for the direct excitation. Fitting was performed using TopSpin 4.0.8 with a Quadrupolar Central transition model and allowed to iterate. $C_Q$ values of each coordination environment were constrained between recycle delay times and are listed in **Table S2**.*

The quadrupolar central transition model (SOlids Lineshape Analysis (SOLA) program of TopSpin 4.0.8) was used for fitting. As only the central transition was excited with a soft pulse, the spinning sideband manifold was not fitted. A Czjzek fit would be more accurate for the amorphous nature of the sample but is unnecessary in the first instance for assessing the recycle delay.

*Table S2 Fitting of the DFS-enhanced Hahn-echo spectra with recycle delays of 75, 225 and 500 ms, with the fractions of each coordination environment present being listed. The fitted value of $C_Q$ for each environment is given and these were kept constrained across each data point.*

| **Coordination site** | **Fraction for each recycle delay (%)** | | |
|---|---|---|---|
| | 75 ms | 225 ms | 500 ms |
| Al(IV) ($C_Q$ = *8.5 MHz*) | 41 | 41 | 30 |
| Al(V) ($C_Q$ = *7.3 MHz*) | 28 | 32 | 33 |
| Al(VI) ($C_Q$ = *3.9 MHz*) | 31 | 28 | 37 |

It should be noted that both the poor signal-to-noise in our spectra and the overlap between the signals will have a significant influence on the confidence in the fitted quantities. While there are deviations of Al(IV):Al(V):Al(VI) quantities between the three recycle delays, the they are within the errors of the fits. When considering the overall build-up of signal intensity from a recycle delay of 75 to 500 ms, the ratio of total intensities for 75 ms:500 ms is approximately 1:1.4. 70 % of the signal was acquired by 75 ms. As the signal-to-noise ratio (SNR) is proportional to the square root of the number of scans, the 75 ms recycle delay is chosen and provides greater SNR (without significant compromise on the quantification) than an experiment with 500 ms for the same experimental time. The proportions of each environment appear different to the spectra of the same sample in **Figure 2** (**a**) due to the higher field at 23.4 T which induces greater broadening of signals with stronger paramagnetic interactions (proportional to the field strength), the shorter pulse lengths used here, and the use of double frequency sweep enhancements where enhancement depends on exciting as many spins in the satellite transitions as possible (sites with different $C_Q$ are less likely to be excited uniformly and thus non-uniform enhancement).[13,14]

## ESI 4: Experimental details for double resonance experiments

$^{27}$Al{$^{1}$H} REDOR was performed at 16.4 T and 50 kHz MAS frequency (1.3 mm rotor) – to determine the appropriate dipolar evolution times, calibration experiments were first performed on $Al(OH)_3$.

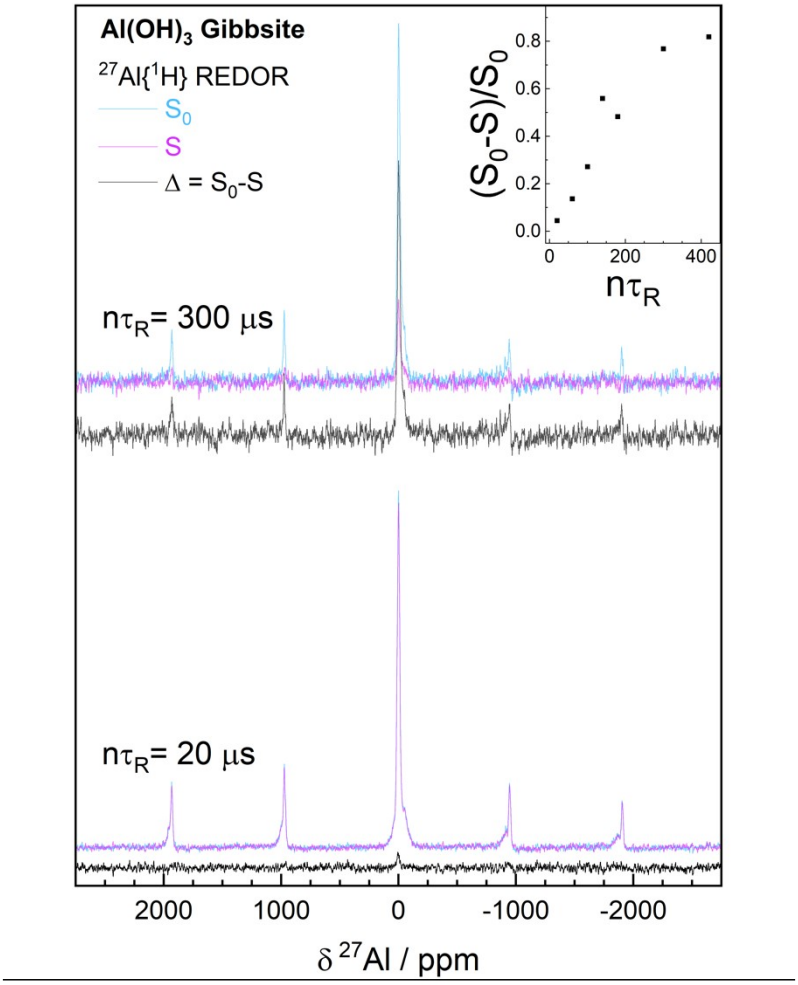


*Figure S2: $^{27}$Al{$^{1}$H} REDOR calibration experiments on gibbsite Al(OH)$_3$ measured at 4.7 T with a recycle delay of 1 s and 50 kHz MAS frequency. $^{27}$Al $\frac{\pi}{6}$ pulses used 156 kHz rf field strength whilst $^{1}$H $\pi$ pulses were excited with 200 kHz. Total dipolar evolution times ($2\tau = n\tau_R$) up to 420 $\mu s$ were probed with the observed REDOR fraction ( $\frac{S - S_0}{S_0}$ ) plotted as function of the total dipolar evolution time in the inset. The spectra without irradiation ($S_0$, cyan) and with irradiation (S, magenta) for two total dipolar evolution times $n\tau_R =$ 20 and 300 $\mu s$ are plotted along with the difference spectrum ($\Delta$, black).*

$^{27}$Al spins were excited with a $\frac{\pi}{6}/\frac{\pi}{3}$ combination (143 kHz rf field strength), $^{1}$H $\pi$ pulses with 152 kHz rf field strength, a 260 $\mu s$ total dipolar evolution period ($2n\tau_D = 2\tau$) and recycle delays of 75 ms for the ALD samples.

$^{1}$H{$^{27}$Al} TRAPDOR was measured directly on the ALD materials. Spectra were acquired at 16.4 T with a 35 kHz MAS frequency (1.3 mm rotor), $^{1}$H excitation with 125 kHz applied rf field strength, $^{27}$Al irradiation with 340 kHz applied rf field strength and a recycle delay of 750 ms. Dipolar evolution times ($\tau$) up to 314 $\mu s$ were probed. In all experiments, the $^{27}$Al carrier frequency was placed in between the Al(VI) and Al(V) resonance frequencies.

Analogous double-resonance REDOR and TRAPDOR experiments were conducted between $^{27}$Al/$^{19}$F and $^{27}$Al/$^{7}$Li. $^{27}$Al{$^{19}$F} REDOR calibration experiments on the reference $\alpha$-$AlF_3$ showed that a total dipolar evolution time of 260 $\mu s$ would allow Al-F dipolar interactions to attenuate ~85 % of the signal intensity of Al in environments with similar Al-F bonds to $AlF_3$.

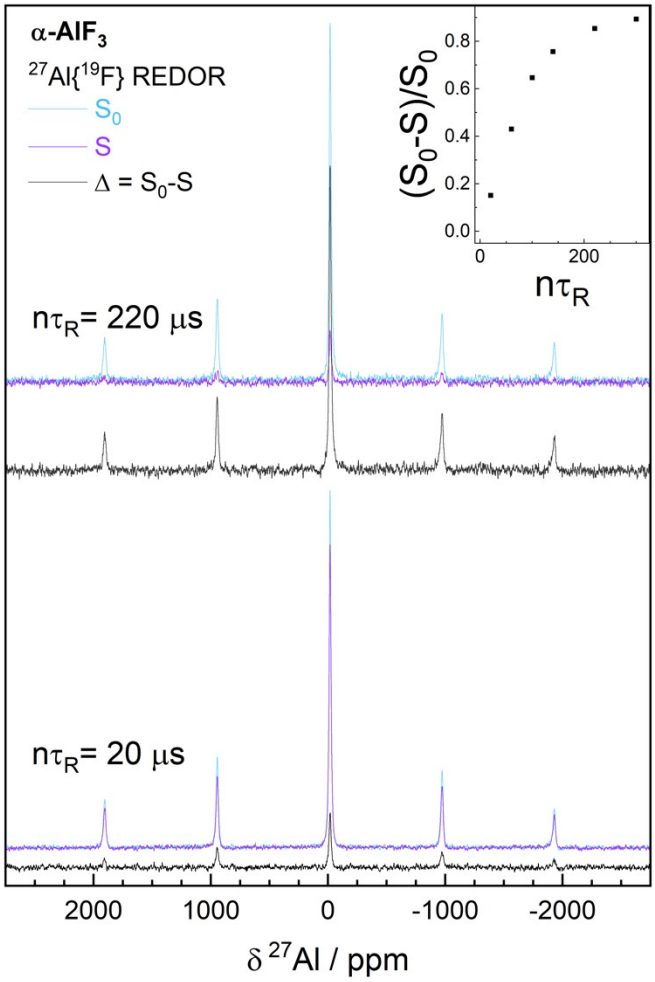


*Figure S3: $^{27}$Al{$^{19}$F} REDOR calibration experiments on $\alpha$-$AlF_3$ measured at 4.7 T with a recycle delay of 1 s and 50 kHz MAS frequency. $^{27}$Al $\frac{\pi}{6}$ pulses used 179 kHz rf field strength whilst $^{19}$F $\pi$ pulses were excited with 200 kHz. Total dipolar evolution times ($2\tau = n\tau_R$) up to 300 $\mu s$ were probed with the observed REDOR fraction ( $\frac{S - S_0}{S_0}$ ) plotted as a function of the total dipolar evolution time in the inset. The spectra without irradiation ($S_0$, cyan) and with irradiation (S, magenta) for two total dipolar evolution times $n\tau_R =$ 20 and 220 $\mu s$ are plotted along with the difference spectrum ($\Delta$, black).*

The $^{19}$F{$^{27}$Al} TRAPDOR calibration experiments on the $\alpha$-$AlF_3$ probed dipolar evolution times up to 225 $\mu s$. The trend in signal attenuation indicates that 25 $\mu s$ is sufficient to see a decrease in signal of about ~16 % under these TRAPDOR conditions.

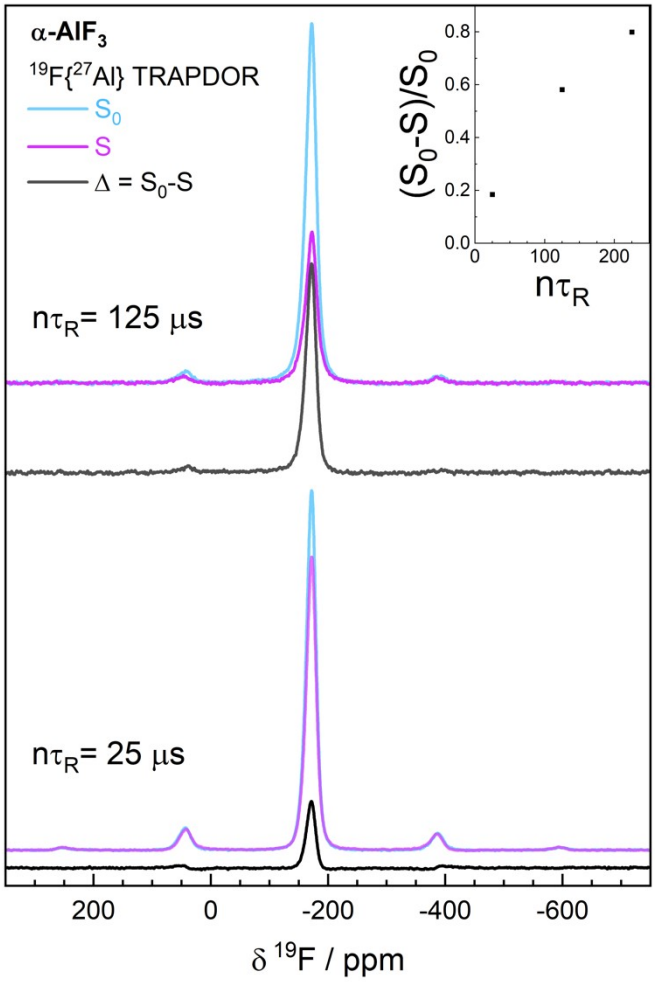


*Figure S4: $^{19}F\{^{27}Al\}$ TRAPDOR calibration experiments on $\alpha$-$AlF_3$ measured at 4.7 T with a recycle delay of 3 s and 40 kHz MAS frequency. $^{19}F$ $\frac{\pi}{2}/\pi$ excitation was achieved with 152 kHz rf field strength whilst $^{27}Al$ adiabatic irradiation used 122 kHz rf field strength. Total dipolar evolution times ($2\tau = n\tau_R$) up to 225 $\mu s$ were probed with the observed TRAPDOR fraction ($\frac{S - S_0}{S_0}$) plotted as function of the total dipolar evolution time in the inset. The spectra without irradiation ($S_0$, cyan) and with irradiation (S, magenta) for two total dipolar evolution times $n\tau_R =$ 25 and 125 $\mu s$ are plotted along with the difference spectrum ($\Delta$, black).*

$^{27}Al\{^{19}F\}$ REDOR experiments on the ALD samples were performed at either 16.4 T (50 kHz MAS frequency, 1.3 mm rotor, $^{27}Al$ excitation with 143 kHz rf field strength, $^{19}F$ excitation with 63 kHz rf field strength, $2\tau$ of 260 $\mu s$ and 75 ms recycle delay) or 23.5 T (26 kHz MAS frequency, 1.9 mm rotor, $^{27}Al$ excitation with 56 kHz rf field strength, $^{19}F$ excitation with 26 kHz rf field strength, $2\tau$ of 290 $\mu s$ and 75 ms recycle delay). All $^{19}F\{^{27}Al\}$ TRAPDOR experiments were measured at 4.7 T with 40 kHz MAS frequency and a 250 ms recycle delay whilst probing $\tau$ up to 175 $\mu s$. A $^{19}F$ rf field strength of 152 kHz was used whilst 122 kHz rf field strength was applied with on the $^{27}Al$ pulse.

$^{27}$Al{$^{7}$Li} REDOR and $^{7}$Li{$^{27}$Al} TRAPDOR experiments were calibrated on a reference $\gamma$-$LiAlO_2$ sample.

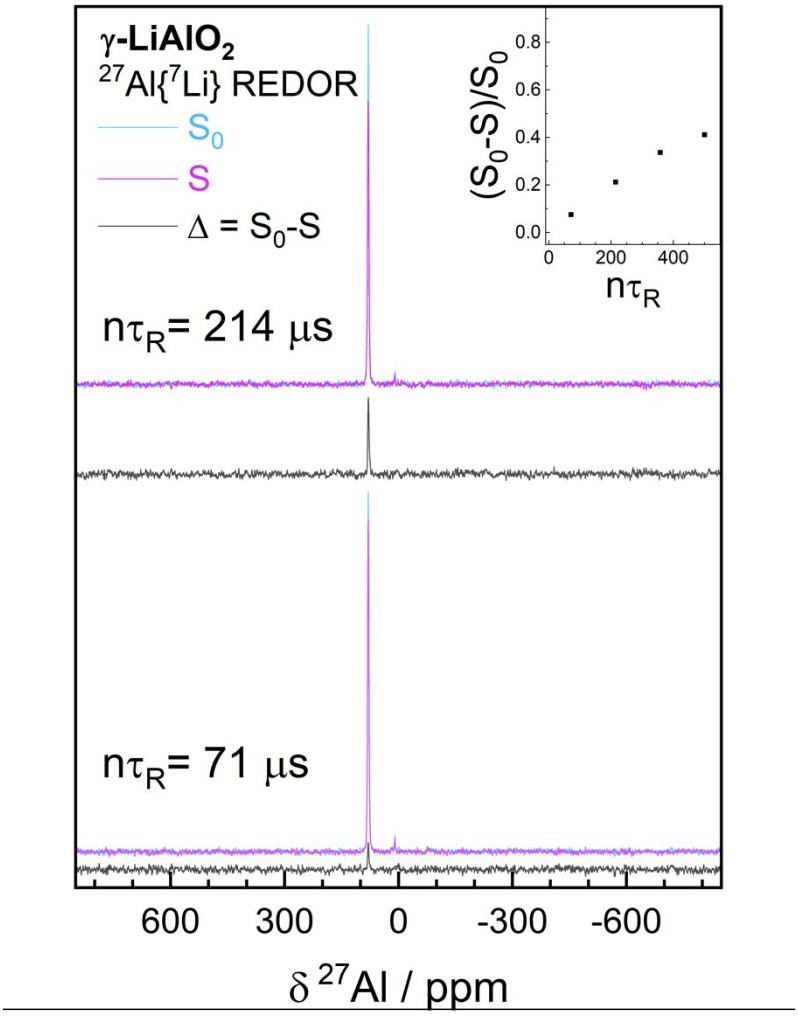


*Figure S5: $^{27}$Al{$^{7}$Li} REDOR calibration experiments on $\gamma$-$LiAlO_2$ measured at 16.4 T with a recycle delay of 50 s and 14 kHz MAS frequency. $^{27}$Al $\frac{\pi}{6}$ pulses used 8 kHz rf field strength whilst $^{7}$Li $\pi$ pulses were excited with 24 kHz. Total dipolar evolution times ($2\tau = n\tau_R$) up to 500 $\mu s$ were probed with the observed REDOR fraction ($\frac{S - S_0}{S_0}$) plotted as function of the total dipolar evolution time in the inset. The spectra without irradiation ($S_0$, cyan) and with irradiation (S, magenta) for two total dipolar evolution times $n\tau_R =$ 71 and 214 $\mu s$ are plotted along with the difference spectrum ($\Delta$, black).*

$^{27}$Al{$^{7}$Li} REDOR on the ALD sample was performed at 16.4 T with a 14 kHz MAS frequency (4.0 mm rotor), 75 ms recycle delay and $2\tau$ of 214 $\mu s$. The $^{27}$Al was excited with 71 kHz rf field strength, 25 kHz rf field strength for the $^{7}$Li.

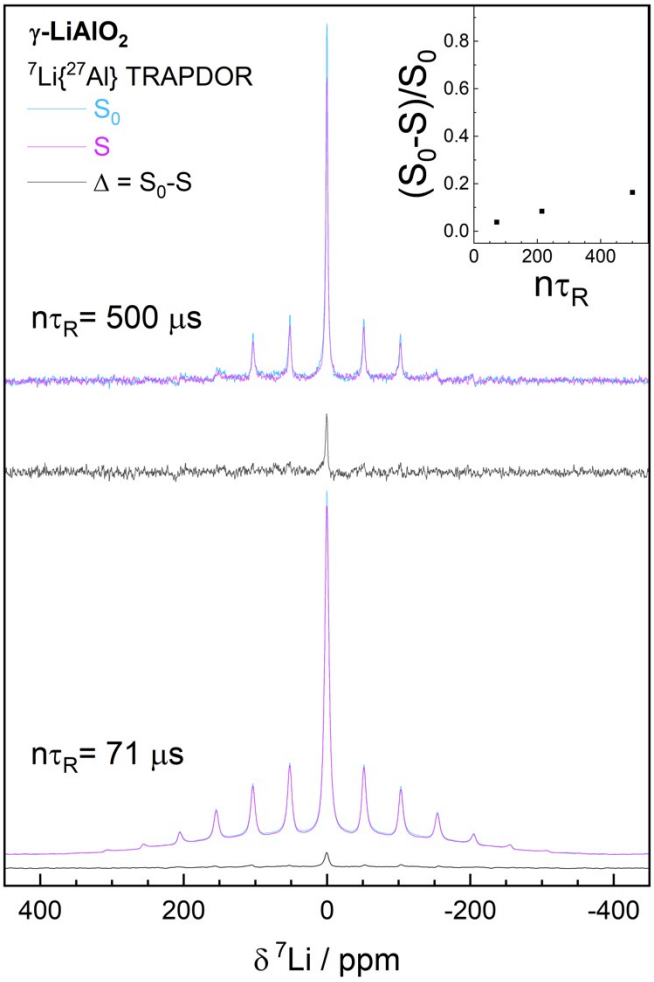


*Figure S6: $^{7}$Li{$^{27}$Al} TRAPDOR calibration experiments on $\gamma$-LiAlO$_2$ measured at 16.4 T with a recycle delay of 30 s and 14 kHz MAS frequency. $^{7}$Li $\frac{\pi}{2}$ pulses used 76 kHz rf field strength whilst the $^{27}$Al adiabatic pulse used 80 kHz. Dipolar evolution times ($\tau = n\tau_R$) up to 500 $\mu s$ were probed with the observed TRAPDOR fraction ( $\frac{S - S_0}{S_0}$ ) plotted as function of the total dipolar evolution time in the inset. The spectra without irradiation ($S_0$, cyan) and with irradiation (S, magenta) for two total dipolar evolution times $n\tau_R =$ 71 and 500 $\mu s$ are plotted along with the difference spectrum ($\Delta$, black).*

$^{7}$Li{$^{27}$Al} TRAPDOR was measured at 16.4 T with a 14 kHz MAS frequency (4.0 mm rotor), 50 ms recycle delay and $\tau$ up to 500 $\mu s$ probed. 38 kHz rf field strength was used for $^{7}$Li excitation whilst 80 kHz rf strength was used for the $^{27}$Al pulse. $^{7}$Li chemical shifts were referenced externally to LiF at (-1 ppm). For all cases, the $^{27}$Al carrier frequency was again placed in between the Al(V) and Al(VI) resonances.

## ESI 5: Supporting NMR experiments

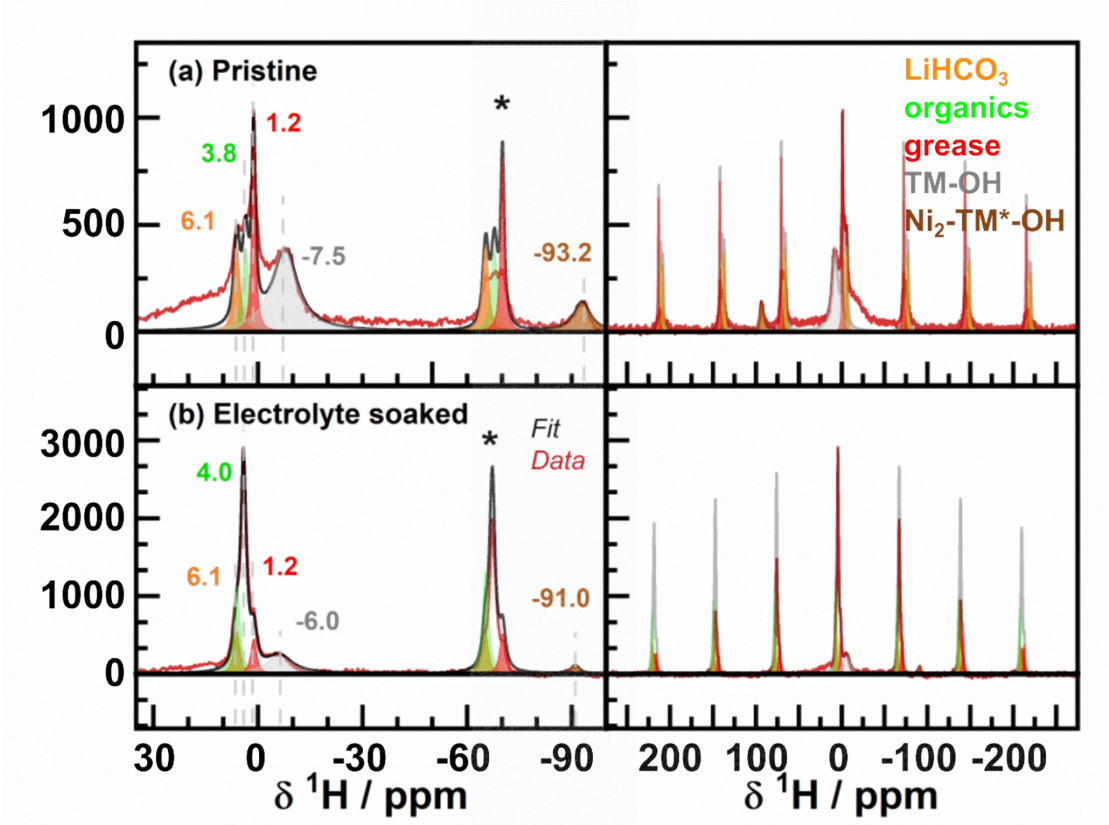


*Figure S7: Normalised (by sample mass and number of scans) $^{1}$H Hahn-echo spectra (after 5 rotor periods of evolution time) of the (a) pristine uncoated NMC811 (narrow spectral window on the LHS and wider range on the RHS) and the (b) electrolyte -soaked uncoated NMC811 (24 h soaking, DMC rinsed) collected at 16.4 T with a spinning frequency of 50 kHz and a recycle delay of 1 s. Fitted using the chemical shift anisotropy model (CSA) of TopSpin that uses Gaussian/Lorentzian line shapes for the isotropic resonance and considers chemical shift anisotropy to fit spinning sidebands.*

To ensure that the $^{1}$H assignments for the $Al_2O_3$ coated materials are not protons bonded to the NMC811, we also measured the pristine uncoated NMC811 and the electrolyte and resonances at 6.1, 3.8 (4.0) and 1.2 ppm within the 0 – 10 ppm range are observed.[15] The most deshielded resonance is tentatively assigned to lithium bicarbonate (6.1 ppm). Soaking the powder in electrolyte results in a dramatic increase in intensity of the 3.8 (4.0) ppm resonance, indicating either organic carbonates or trace water from the electrolyte likely physisorbs onto the NMC811 surface. The pristine uncoated NMC811 are exposed to volatile organic carbonates in the Ar glovebox environment. Another resonance is also observed at 1.2 ppm. LiOH is shown to have a range of shifts from -1.5 – -1.0 ppm. depending on the degree of crystallinity so would not explain the resonance at 1.2 ppm.[16] $^{1}$H resonances at ~-3 ppm have been recorded for some Ni(II) complexes for terminal OH groups without hydrogen bonding.[17] The unknown resonance at -7.5 (-6.0) ppm could therefore be assigned to terminal groups of transition metal cations in the TM layer whilst the resonances at 1.2 ppm are more likely organic impurities such as grease.

Spinning sidebands spanning >400 ppm (>280 kHz at 16.4 T) and symmetric distribution of sideband intensities indicates the influence of strong dipolar interactions (or paramagnetic interactions). As such, chemical shielding anisotropy is required in the fitting to model the sidebands. However, this is only an approximation - the iterated $\delta_{CSA}$ and $\eta_{CSA}$ parameters are never able to accurately fit the sideband intensities.

*Table S3 Fitting of the $^1$H Hahn-echo spectrum of the pristine NMC811 collected at 16.4 T with the fitted values for $\delta_{iso}$, $\delta_{CSA}$, $\eta_{CSA}$, Lorentzian and Gaussian broadening parameters in the chemical shift anisotropy model of TopSpin.*

| Pristine NMC811 | | | | |
|---|---|---|---|---|
| $\delta_{iso}$ / ppm | $\delta C_{SA}$ / ppm | $\eta_{CSA}$ | Lorent. broad. / Hz | Gauss. broad. / Hz |
| 6.059 | 1578.3 | 0.970 | 1200 | 600 |
| 3.754 | 1393.2 | 0.924 | 1200 | 600 |
| 1.223 | 1282.3 | 0.991 | 800 | 300 |
| -7.466 | - | - | 6000 | 600 |
| -92.984 | - | - | 3800 | 600 |

*Table S4 Fitting of the $^1$H Hahn-echo spectrum of the NMC811 soaked in electrolyte, collected at 16.4 T with the fitted values for $\delta_{iso}$, $\delta_{CSA}$, $\eta_{CSA}$, Lorentzian and Gaussian broadening parameters in the chemical shift anisotropy model of TopSpin.*

| Electrolyte soaked NMC811 | | | | |
|---|---|---|---|---|
| $\delta_{iso}$ / ppm | $\delta C_{SA}$ / ppm | $\eta_{CSA}$ | Lorent. broad. / Hz | Gauss. broad. / Hz |
| 6.100 | 1104.2 | 0.997 | 1200 | 600 |
| 4.041 | 1103.7 | 0.997 | 1200 | 400 |
| 1.187 | 987.4 | 0.853 | 1100 | 600 |
| -6.000 | - | - | 6000 | 1000 |
| -91.000 | - | - | 2000 | 0 |

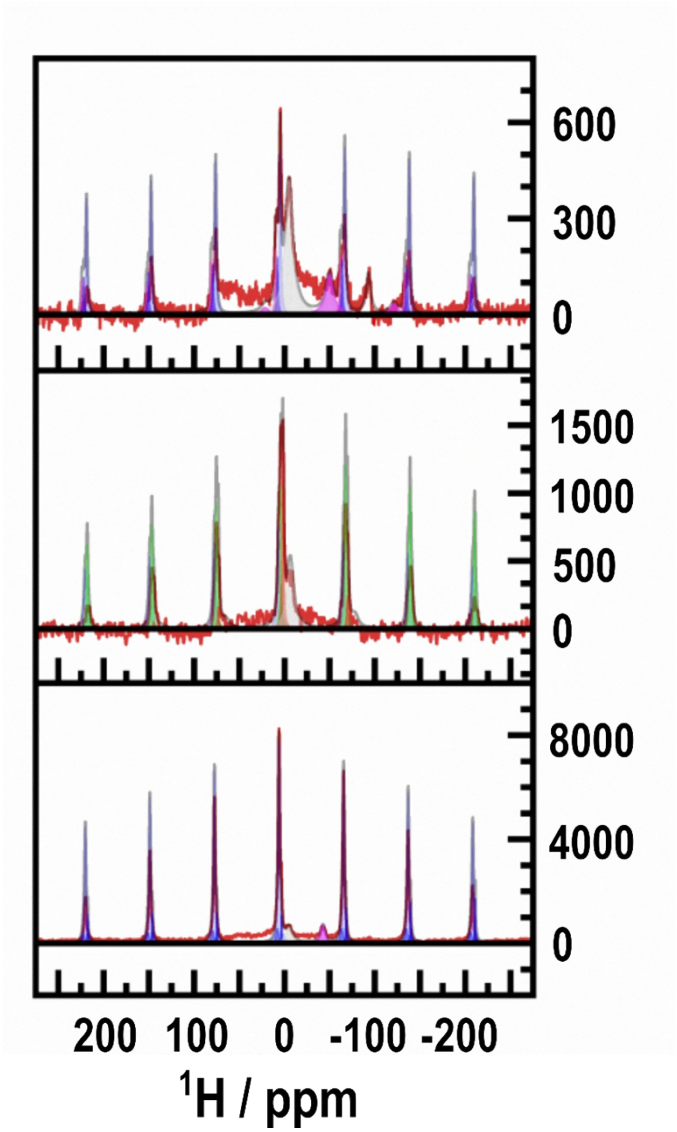


*Figure S8: Mass normalised ¹H Hahn-echo spectra of the ALD NMC811 samples in the (a) pristine state, (b) EC/EMC soaked state and (c) electrolyte soaked state. Wide view shows the spinning sidebands of the spectra and the limitations of the Gaussian/Lorentzian fitting with chemical shift anisotropy considered. Sidebands are overfitted in intensity with the model but without the CSA parameters, sidebands are not fit at all.*

*Table S5 Fitting of the ¹H Hahn-echo spectrum of the pristine ALD NMC811 collected at 16.4 T with the fitted values for $\delta_{iso}$, $\delta_{CSA}$, $\eta_{CSA}$, Lorentzian and Gaussian broadening parameters in the chemical shift anisotropy model of TopSpin.*

| Pristine ALD NMC811 | | | | |
|---|---|---|---|---|
| | | | Lorent. broad. | Gauss. broad. |
| $\delta_{iso}$ / ppm | $\delta C_{SA}$ / ppm | $\eta_{CSA}$ | / Hz | / Hz |
| 9.496 | 475.87 | 0.895 | 1200 | 600 |
| 7.527 | 1109.80 | 0.957 | 1200 | 600 |
| 4.523 | 2120.33 | 0.955 | 1200 | 800 |
| -5.161 | - | - | 7000 | 1285 |
| -50.000 | - | - | 7000 | 600 |
| -93.000 | - | - | 4000 | 600 |

*Table S6: Fitting of the $^{1}$H Hahn-echo spectrum of the EC/EMC soaked ALD NMC811 collected at 16.4 T with the fitted values for $\delta_{iso}$, $\delta_{CSA}$, $\eta_{CSA}$, Lorentzian and Gaussian broadening parameters in the chemical shift anisotropy model of TopSpin.*

| EC/EMC soaked ALD NMC811 | | | | |
|---|---|---|---|---|
| $\delta_{iso}$ / ppm | $\delta C_{SA}$ / ppm | $\eta_{CSA}$ | Lorent. broad. / Hz | Gauss. broad. / Hz |
| 5.954 | 814.76 | 0.988 | 2000 | 600 |
| 3.620 | 984.30 | 0.864 | 1200 | 600 |
| 1.521 | 174.63 | 0.858 | 1200 | 600 |
| -6.656 | - | - | 6000 | 800 |

*Table S7: Fitting of the $^{1}$H Hahn-echo spectrum of the electrolyte soaked ALD NMC811 collected at 16.4 T with the fitted values for $\delta_{iso}$, $\delta_{CSA}$, $\eta_{CSA}$, Lorentzian and Gaussian broadening parameters in the chemical shift anisotropy model of TopSpin.*

| Electrolyte-soaked ALD NMC811 | | | | |
|---|---|---|---|---|
| $\delta_{iso}$ / ppm | $\delta C_{SA}$ / ppm | $\eta_{CSA}$ | Lorent. broad. / Hz | Gauss. broad. / Hz |
| 7.700 | 1108.89 | 0.903 | 2000 | 800 |
| 5.805 | 843.69 | 0.992 | 1400 | 600 |
| 3.104 | 1707.27 | 0.669 | 600 | 100 |
| -5.000 | - | - | 6000 | 800 |
| -42.700 | - | - | 4000 | 600 |

*Table S8: Fitting of the $^{27}$Al Hahn-echo spectrum of the pristine ALD NMC811 collected at 23.4 T with the fitted values for $\delta_{iso}$, $C_Q$ and the phase fraction of each environment is presented.*

| Pristine ALD NMC811 | | | |
|---|---|---|---|
| Coordination site | $\delta_{iso}$ / ppm | $C_Q$ / MHz | Fraction / % |
| 4 | 82.5 | 15.7 | 47 |
| 5 | 46.5 | 15.7 | 37 |
| 6 | 16.7 | 12.6 | 16 |

A Czjzek model is used to fit the spectrum as the presence of the Al (V) environment suggests a disordered/amorphous system – the Czjzek model on dmfit allows simulation of a distribution of quadrupolar interactions unlike quadrupolar models on programs like TopSpin.[18,19] As such only the average $C_Q$ and the isotropic chemical shift ($\delta_{iso}$) determined from the fits are reported – other typical quadrupolar properties like the asymmetry parameter are not included in the model due to the distribution of quadrupolar properties (and hence an observed peak with no well-defined lineshape typical of quadrupolar nuclei).

*Table S9: Fitting of the $^{27}$Al Hahn-echo spectrum of the EC/EMC soaked ALD NMC811 collected at 16.4 T with the fitted values for $\delta_{iso}$, $C_Q$ and the phase fraction for each environment presented.*

| EC/EMC soaked ALD NMC811 | | | |
|---|---|---|---|
| Coordination site | $\delta_{iso}$ / ppm | $C_Q$ / MHz | Fraction / % |
| 4 | 78.4 | 9.1 | 36 |
| 5 | 46.0 | 9.0 | 25 |
| 6 | 14.2 | 6.7 | 39 |

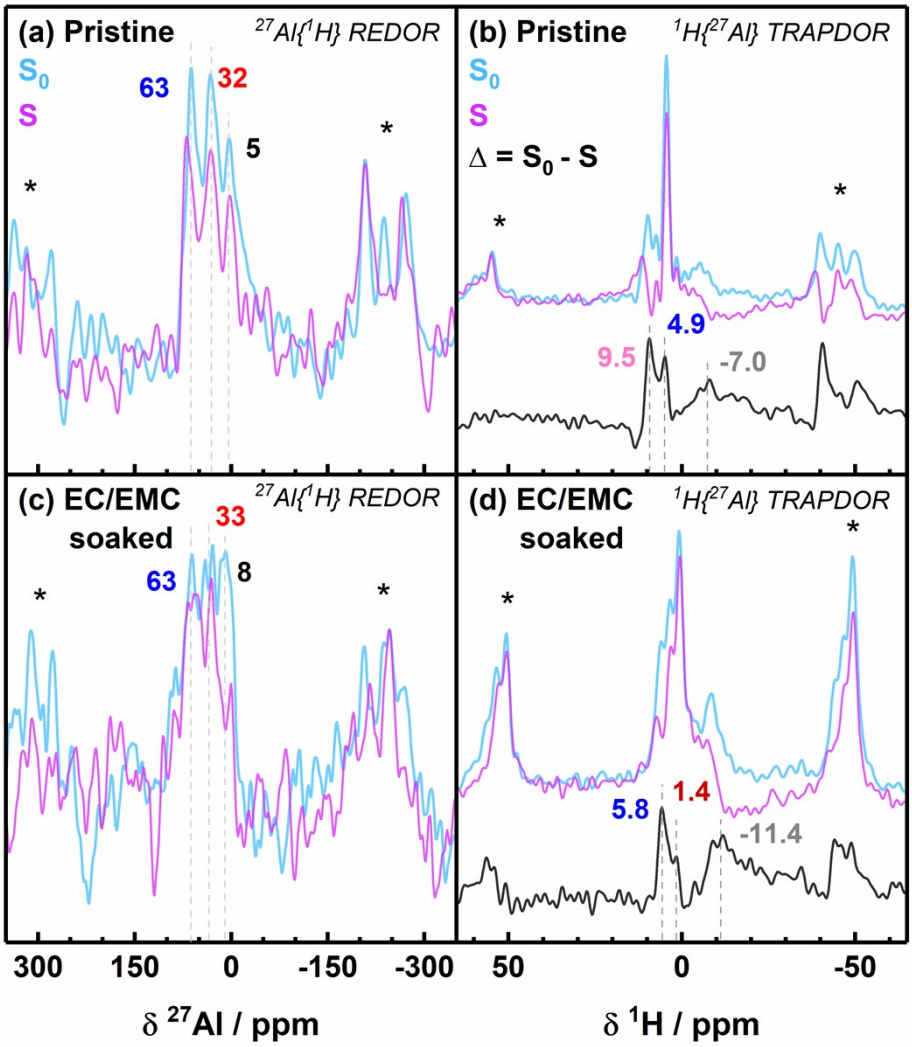


*Figure S9: Double-resonance experiments on the (a-b) pristine ALD NMC811 and (c-d) the material after soaking in EC/EMC solvent. $^{27}$Al observed REDOR experiments (a and c) without $^{1}$H irradiation ($S_0$, cyan) during a total dipolar evolution time of 260 $\mu s$ and with $^{1}$H $\pi$ pulses (S, magenta) during this total dipolar evolution time are given – regions of attenuated signal indicate $^{1}$H spin in proximity to $^{27}$Al. Spectra were acquired at 16.4 T with 50 kHz MAS frequency and 75 ms recycle delays. $^{1}$H observed TRAPDOR experiments (b and d) without $^{27}$Al irradiation ($S_0$, cyan) over a dipolar evolution period of 260 $\mu s$ and with $^{27}$Al adiabatic irradiation (S, purple, 340 kHz rf) for this dipolar evolution time are plotted. The difference spectrum ($\Delta$, black) is also plotted to highlight the $^{1}$H resonances that experience dipolar interactions with nearby $^{27}$Al spins. Spectra were acquired at 16.4 T with 35 kHz MAS frequency and 1 s recycle delays. Spinning sidebands are denoted with asterisks (*).*

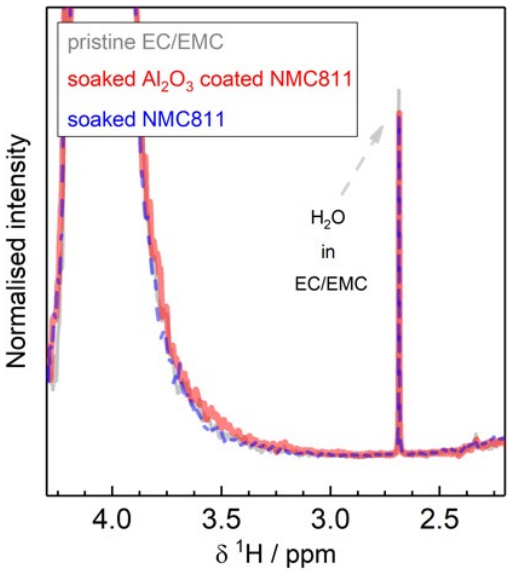


*Figure S10: $^1$H NMR of pristine EC/EMC solvent (grey), EC/EMC after soaking $Al_2O_3$ coated NMC811 for 24 h (red) and EC/EMC after soaking uncoated NMC811 for 24 h (blue dash). A sealed capillary of $C_6D_6$ was used for external shift referencing. Spectra were normalised to the peak intensity of EC.*

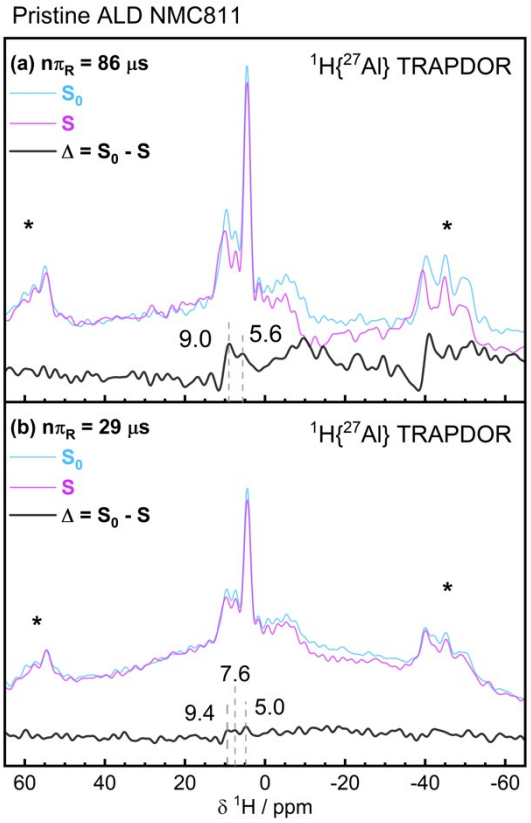


*Figure S11: $^1$H{$^{27}$Al} TRAPDOR experiments on the pristine ALD NMC811 material for (a) 29 $\mu s$ and (b) 86 $\mu s$ of total dipolar evolution times. The experiment without $^{27}$Al irradiation ($S_0$, cyan) over the dipolar evolution period and with $^{27}$Al adiabatic irradiation (S, purple, 340 kHz rf) for this dipolar evolution time are plotted. $^1$H was excited with 125 kHz rf field strength. The difference spectrum ($\Delta$, black) is also plotted to highlight the $^1$H resonances that experience dipolar interactions with nearby $^{27}$Al spins. Spectra were acquired at 16.4 T with 35 kHz MAS frequency and 1 s recycle delays. Spinning sidebands are denoted with asterisks (*).*

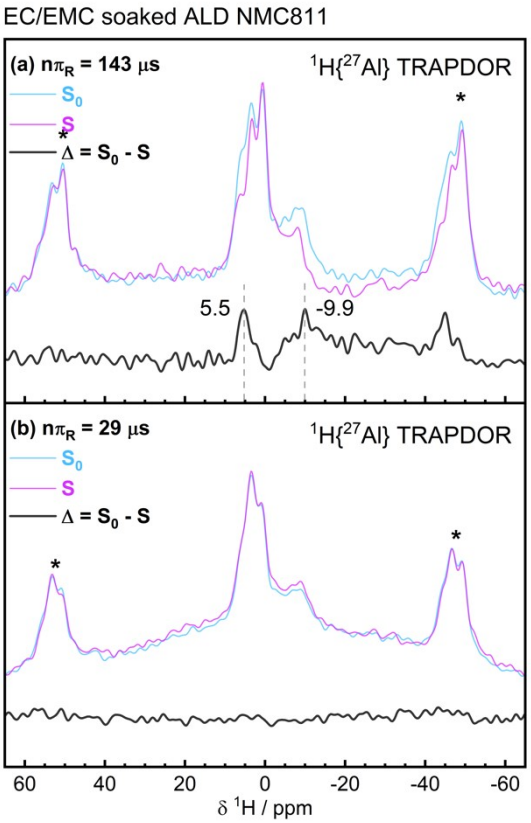


*Figure S12: $^{1}H\{^{27}Al\}$ TRAPDOR experiments on the ALD NMC811 material soaked in EC/EMC solvent after rinsing with DMC (and dried in-vacuo) for (a) 29 $\mu s$ and (b) 143 $\mu s$ of total dipolar evolution times. The experiment without $^{27}Al$ irradiation ($S_0$, cyan) over the dipolar evolution period and with $^{27}Al$ adiabatic irradiation (S, purple, 340 kHz rf) for this dipolar evolution time are plotted. $^{1}H$ was excited with 125 kHz rf field strength. The difference spectrum ( $\Delta$, black) is also plotted to highlight the $^{1}H$ resonances that experience dipolar interactions with nearby $^{27}Al$ spins. Spectra were acquired at 16.4 T with 35 kHz MAS frequency and 1 s recycle delays. Spinning sidebands are denoted with asterisks (*).*

*Table S10 Fitting of the $^{27}Al$ Hahn-echo spectrum of the electrolyte-soaked ALD NMC811 collected at 16.4 T with the fitted values for $\delta_{iso}$, $C_Q$ and the phase fraction for each environment presented.*

| Electrolyte-soaked ALD NMC811 | | | |
|---|---|---|---|
| Coordination site | $\delta_{iso}$ / ppm | $C_Q$ / MHz | Fraction / % |
| Al (IV) | 62.9 | 7.9 | 31 |
| Al (V) | 38.3 | 9.9 | 30 |
| Al (VI) | 3.6 | 6.4 | 39 |

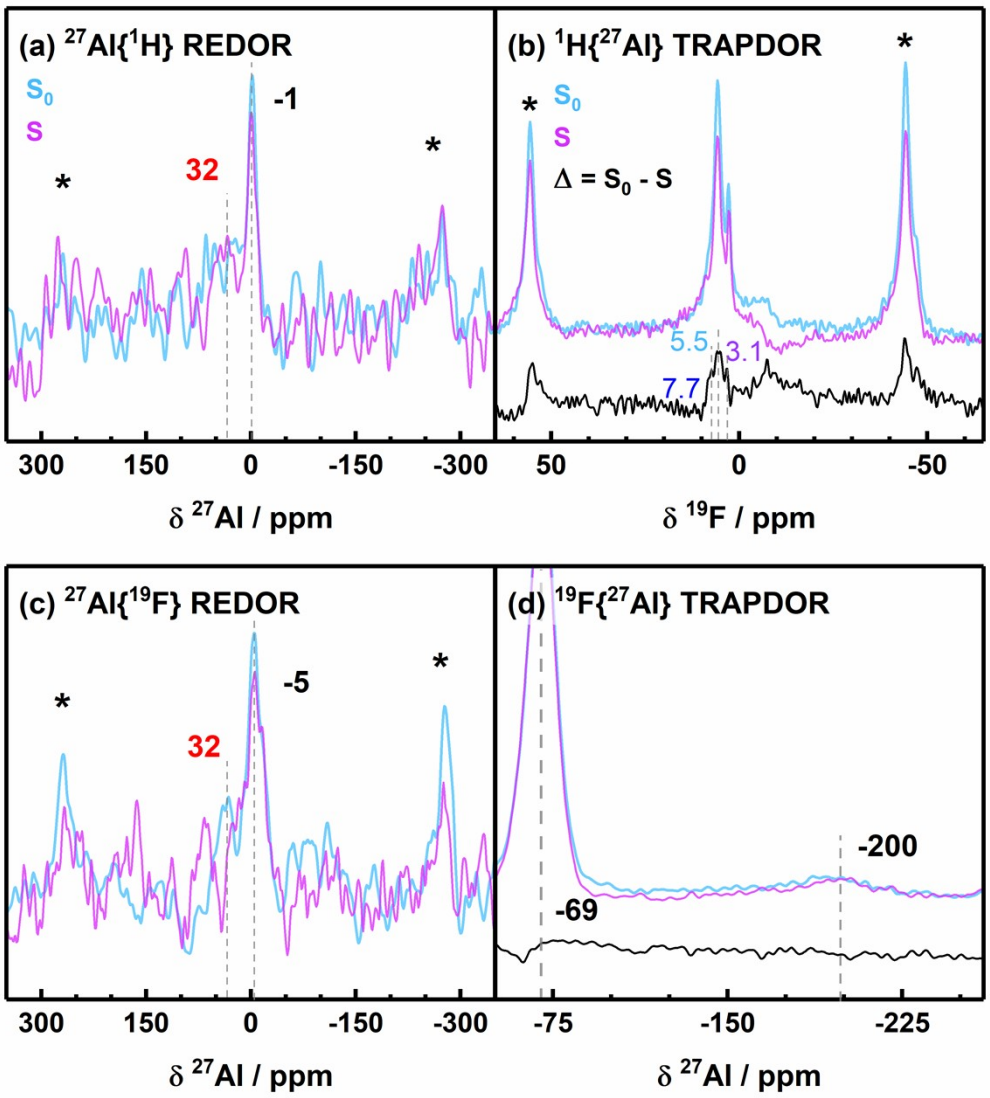


*Figure S13: Double-resonance experiments on the ALD NMC811 soaked in 1 M $LiPF_6$ in EC/EMC (3/7 (v/v)) after rinsing with DMC (and dried in-vacuo). In (a) is the $^{27}Al\{^{1}H\}$ REDOR experiment without $^{1}H$ irradiation ($S_0$, cyan) during a total dipolar evolution time of 260 $\mu s$ and with $^{1}H$ $\pi$ pulses (S, magenta) during this total dipolar evolution time are given. Attenuated signal indicates $^{1}H$ spins in proximity to $^{27}Al$. Spectra were acquired at 16.4 T with 50 kHz MAS frequency and 75 ms recycle delays. In (b) the $^{1}H\{^{27}Al\}$ TRAPDOR without $^{27}Al$ irradiation ($S_0$, cyan) over a dipolar evolution period of 260 $\mu s$ and with $^{27}Al$ adiabatic irradiation (S, purple, 340 kHz rf) for this dipolar evolution time are plotted. The difference spectrum ($\Delta$, black) is also plotted to highlight the $^{1}H$ resonances that experience dipolar interactions with nearby $^{27}Al$ spins. Spectra were acquired at 16.4 T with 35 kHz MAS frequency and 1 s recycle delays. In (c) is the $^{27}Al\{^{19}F\}$ REDOR experiment without $^{19}F$ irradiation ($S_0$, cyan) during a total dipolar evolution time of 260 $\mu s$ and with $^{19}F$ $\pi$ pulses (S, magenta). Spectra were acquired at 16.4 T with 50 kHz MAS frequency and 75 ms recycle delays. In (d) is the $^{19}F\{^{27}Al\}$ TRAPDOR experiment without $^{27}Al$ irradiation ($S_0$, cyan) during a total dipolar evolution time of 25 $\mu s$ and with $^{27}Al$ adiabatic irradiation (S, purple, 122 kHz rf) to yield a difference spectrum ($\Delta$, black). Spectra were acquired at 4.7 T with 40 kHz MAS frequency and 250 ms recycle delays. Spinning sidebands are denoted with asterisks (*).*

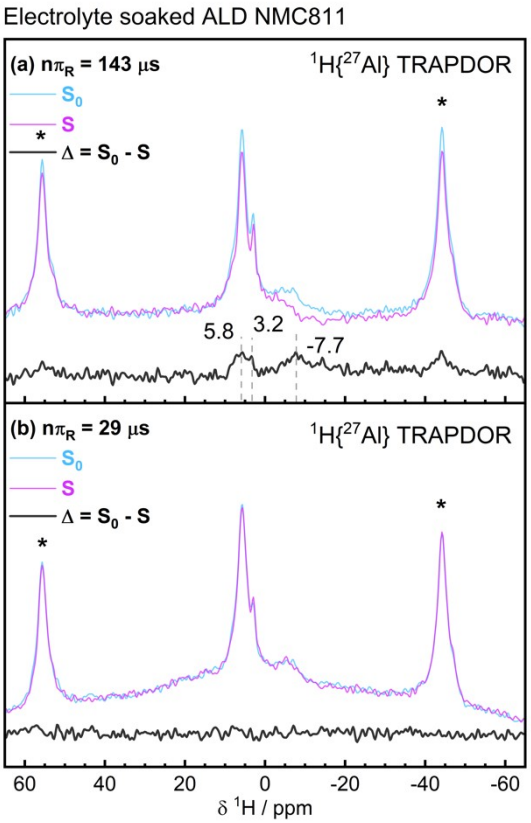


*Figure S14: $^{1}H\{^{27}Al\}$ TRAPDOR experiments on the ALD NMC811 material soaked in 1 M $LiPF_6$ in EC/EMC (3/7 (v/v)) after rinsing with DMC (and dried in-vacuo) for (a) 29 $\mu s$ and (b) 143 $\mu s$ of total dipolar evolution times. The experiment without $^{27}Al$ irradiation ($S_0$, cyan) over the dipolar evolution period and with $^{27}Al$ adiabatic irradiation (S, purple, 340 kHz rf) for this dipolar evolution time are plotted. $^{1}H$ was excited with 125 kHz rf field strength. The difference spectrum ($\Delta$, black) is also plotted to highlight the $^{1}H$ resonances that experience dipolar interactions with nearby $^{27}Al$ spins. Spectra were acquired at 16.4 T with 35 kHz MAS frequency and 1 s recycle delays. Spinning sidebands are denoted with asterisks (*).*

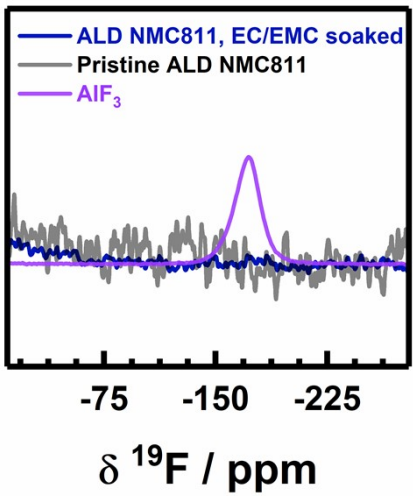


*Figure S15: Mass-normalised $^{19}F$ MAS NMR spectra of the ALD NMC811 powders in the as-synthesised pristine state (black) and after soaking in EC/EMC solvent (blue, also rinsed with DMC before drying in-vacuo). Spectra were collected at 4.7 T, with 50 kHz MAS frequency and a 250 ms recycle delay. Reference $AlF_3$ was also recorded.*

The $^{19}F$ spectra of $LiPF_6$-free samples indicates that all the $^{19}F$ resonances observed in **Figure 3 (b)** must come from reactions between the NMC811 (with/without the $Al_2O_3$) and species in the $LiPF_6$ containing electrolyte.

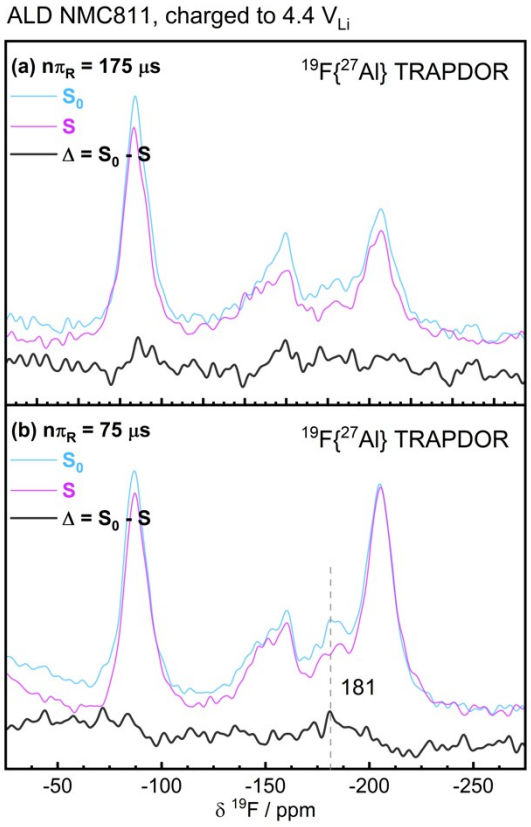


*Figure S16: $^{19}F\{^{27}Al\}$ TRAPDOR experiments on the ALD NMC811 material charged up to 4.4 $V_{Li}$ (sample II) after rinsing with DMC (and dried in-vacuo) for (a) 75 $\mu s$ and (b) 175 $\mu s$ of total dipolar evolution times. The experiment without $^{27}Al$ irradiation ($S_0$, cyan) over the dipolar evolution period and with $^{27}Al$ adiabatic irradiation (S, purple, 122 kHz rf) for this dipolar evolution time are plotted. $^{19}F$ was excited with 152 kHz rf field strength. The difference spectrum ($\Delta$, black) is also plotted to highlight the $^{1}H$ resonances that experience dipolar interactions with nearby $^{27}Al$ spins. Spectra were acquired at 4.7 T with 40 kHz MAS frequency and 250 ms recycle delays.*

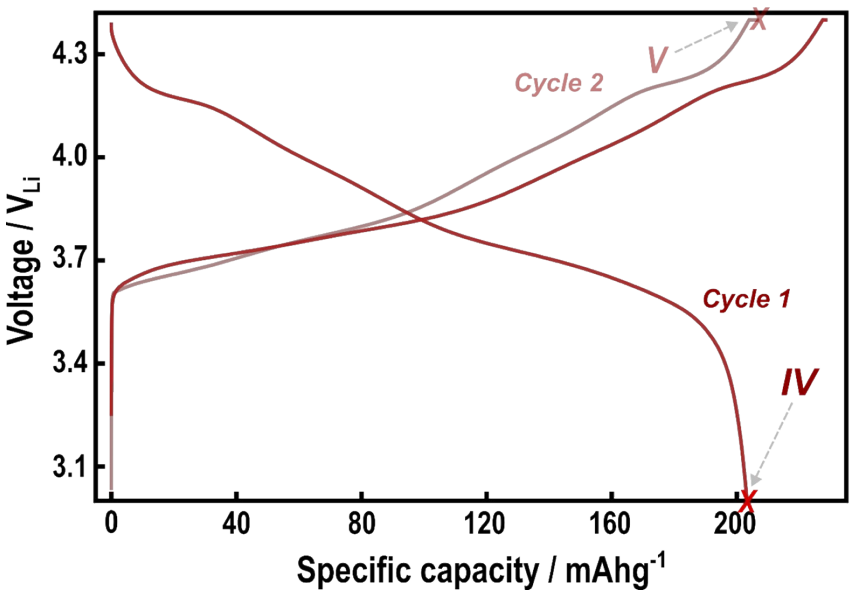


*Figure S17: Voltage profile of ALD NMC811 in binder-free Swagelok cells for cycle 1 (opaque, IV) and 2 (transparent, V). The cycle 1 sample was left in the discharged state (3.0 $V_{Li}$) whilst the cycle 2 sample was left in the charged state (4.4 $V_{Li}$). Cells were cycled at a C/20 rate assuming 200 $mAhg^{-1}$ practical capacity between 3.0 – 4.4 $V_{Li}$ with a voltage hold at 4.4 $V_{Li}$ until the current decays to an equivalent of C/40 value.*

*Table S11 Fitting of the $^{27}Al$ Hahn-echo spectrum of the ALD NMC811 charged to 4.4 $V_{Li}$ collected at 23.4 T with the fitted values for $\delta_{iso}$, $C_Q$ and the phase fraction for each environment presented.*

| ALD NMC811, charged to 4.4 $V_{Li}$ | | | |
|---|---|---|---|
| Coordination site | $\delta_{iso}$ / ppm | $C_Q$ / MHz | Fraction / % |
| Al (IV) ii | 74.5 | 12.0 | 17 |
| Al (IV) i | 60.6 | 10.6 | 24 |
| Al (V) | 38.0 | 13.2 | 27 |
| Al (VI) | 5.9 | 9.0 | 32 |

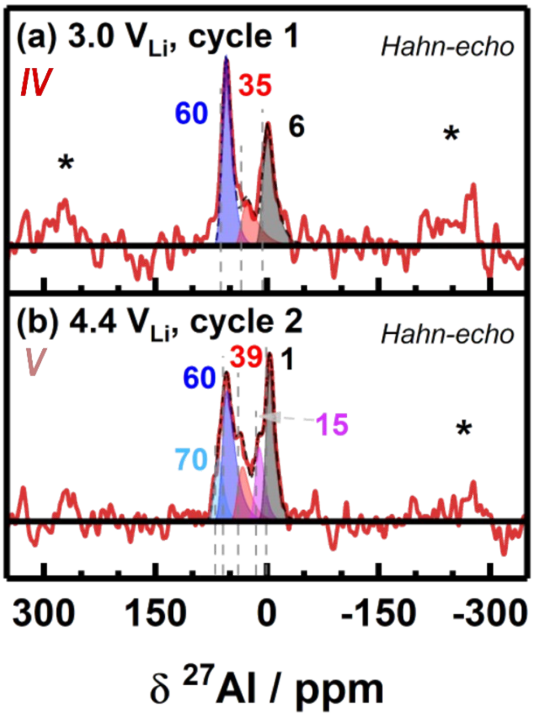


*Figure S18: $^{27}$Al MAS NMR spectra of the cycled ALD NMC811 after rinsing with DMC. In (a), the material is discharged to 3.0 $V_{Li}$ after 1 cycle (point IV, 3.0 – 4.4 $V_{Li}$ charged at C/20 assuming a 200 mAhg$^{-1}$ practical capacity) whilst in (b) is the material charged back to 4.4 $V_{Li}$ after the first cycle (point V, 3.0 – 4.4 $V_{Li}$, C/20 rate). The spectra are acquired with a Hahn-Echo pulse sequence at 16.4 T with a 50 kHz MAS frequency and 75 ms recycle delay. Spectra are fitted using a Czjzek model; the tetrahedral Al(IV), pentahedral Al(V) and octahedral Al(VI) components are plotted in blue (and cyan), red and black (and purple) respectively. Isotropic chemical shifts of each fitted component are marked with a dashed line. Spinning sidebands are marked with asterisks (*).*

*Table S12 Fitting of the $^{27}$Al Hahn-echo spectrum of the ALD NMC811 in the discharged state after cycling from 3 – 4.4 $V_{Li}$ collected at 16.4 T with the fitted values for $\delta_{iso}$, $C_Q$ and the phase fraction for each environment presented.*

| ALD NMC811, discharged to 3.0 $V_{Li}$ | | | |
|---|---|---|---|
| Coordination site | $\delta_{iso}$ / ppm | $C_Q$ / MHz | Fraction / % |
| 4 | 60.2 | 6.1 | 48 |
| 5 | 35.2 | 9.0 | 18 |
| 6 | 6.0 | 7.3 | 34 |

*Table S13: Fitting of the $^{27}$Al Hahn echo spectrum of the ALD NMC811 charged to 4.4 $V_{Li}$ on cycle 2 collected at 16.4 T with the fitted values for $\delta_{iso}$, $C_Q$ and the phase fraction for each environment presented.*

| ALD NMC811, charged to 4.4 $V_{Li}$ on cycle 2 | | | |
|---|---|---|---|
| Coordination site | $\delta_{iso}$ / ppm | $C_Q$ / MHz | Fraction / % |
| Al (IV) ii | 70.4 | 5.7 | 33 |
| Al (IV) i | 60.5 | 7.6 | 11 |
| Al (V) | 39.9 | 7.6 | 14 |
| Al (VI) ii | 15.3 | 5.8 | 28 |
| Al (VI) i | 0.8 | 5.7 | 14 |

A $^{7}$Li{$^{27}$Al} TRAPDOR experiment was first performed for a reference $\gamma$-$LiAlO_2$ sample so as to optimise the conditions required to observe $^{7}$Li{$^{27}$Al} dipolar coupling. The $^{7}$Li signal of this sample at 0.5 ppm is readily attenuated ($^{7}$Li{$^{27}$Al} TRAPDOR in **Figure S19** (**a**)) when $^{27}$Al irradiation is applied for 214 $\mu s$.

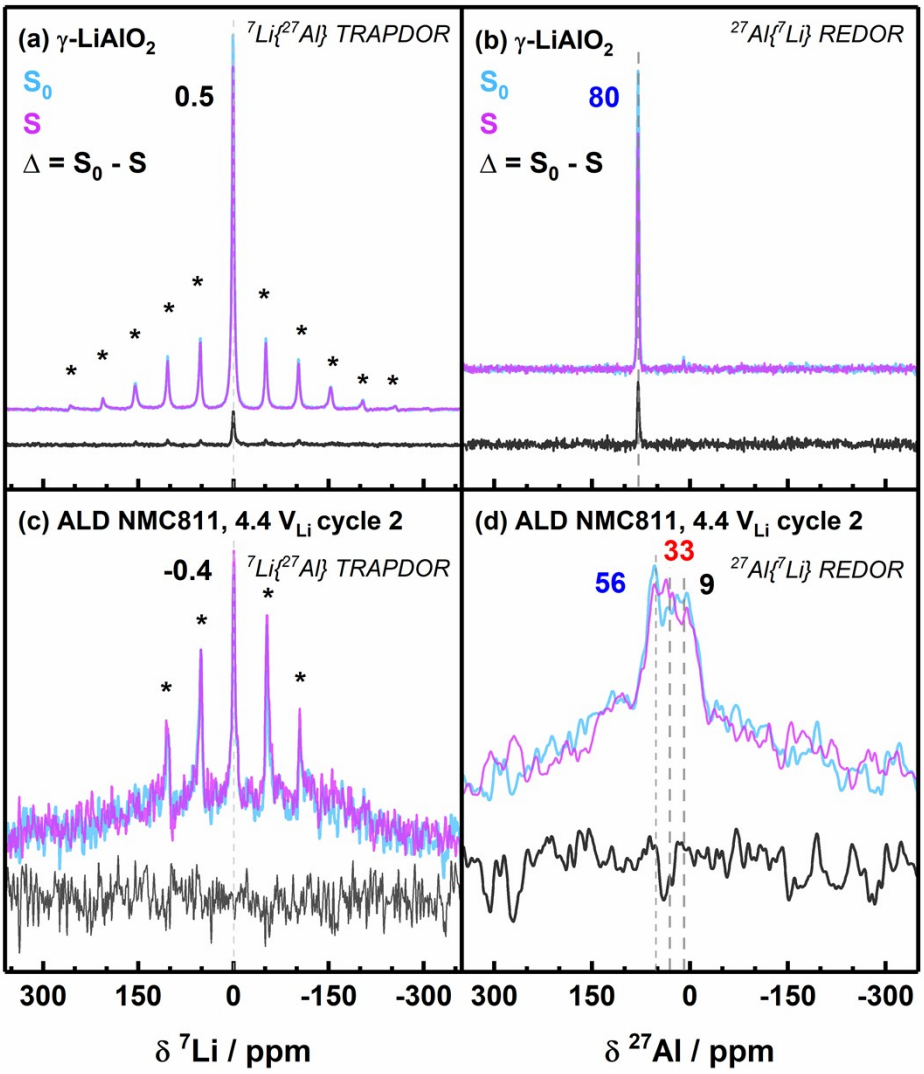


*Figure S19: $^{7}$Li-$^{27}$Al double resonance experiments (16.4 T, 14 kHz MAS spinning) comparing $\gamma$-$LiAlO_2$ (a – b) and the ALD NMC811 charged back to 4.4 $V_{Li}$ after one cycle (c – d). The $^{7}$Li{$^{27}$Al} TRAPDOR experiments (a, c) without $^{27}$Al irradiation ($S_0$, cyan) is compared to the experiment with $^{27}$Al irradiation (S, magenta) to give a difference spectrum ($\Delta$, black). The dipolar evolution time for the recoupling is 214 $\mu s$ for (a) the $\gamma$-$LiAlO_2$ and 286 $\mu s$ for (c) the charged ALD NMC811 material. $^{27}$Al{$^{7}$Li} REDOR experiments (b, d) without $^{7}$Li irradiation ($S_0$, cyan) is compared to the experiment with $^{7}$Li irradiation (S, magenta) to give a difference spectrum ($\Delta$, black). The dipolar dipolar evolution time for the recoupling is 214 $\mu s$ for both (b) the $\gamma$-$LiAlO_2$ and (d) the charged ALD NMC811. Spinning sidebands are marked with asterisks (*).*

$^{7}$Li{$^{27}$Al} TRAPDOR of the cycled, ALD sample shows little reduction in the diamagnetic and isotropic $^{7}$Li signal after $^{27}$Al irradiation (80 kHz rf field strength) over 286 $\mu s$ (four rotor periods) of dipolar evolution time. In comparison, the $\gamma$-$LiAlO_2$ at the same spinning speeds and applied $^{27}$Al rf pulse shows a much more obvious signal attenuation within 214 $\mu s$ (3 rotor periods). This suggests that the dipolar interactions between $^{7}$Li and $^{27}$Al in the cycled

ALD NMC811 are much weaker than in $\gamma$-$LiAlO_2$ and different diamagnetic Li environments are present in the ALD material given the different chemical shifts.

$^{27}Al\{^{7}Li\}$ REDOR experiments of the same $\gamma$-$LiAlO_2$ and the ALD NMC811 samples support the TRAPDOR results – little attenuation of $^{27}Al$ resonances is observed despite the same MAS frequency and total dipolar evolution periods being tested.

## ESI 6: Additional evidence of the coating stabilising the surface O

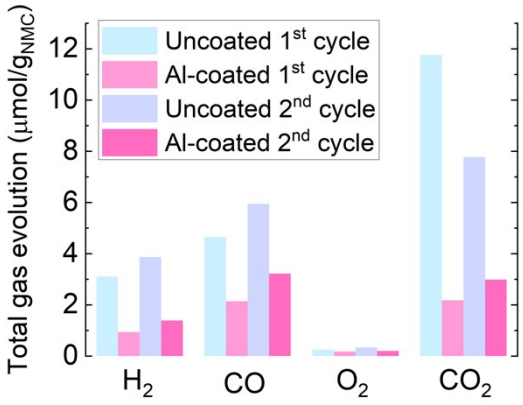


*Figure S20: Total gas evolution of the operando cells normalised by the mass of NMC811 for $H_2$, CO, $O_2$ and $CO_2$ during the first two cycles. Operando cells are cycled between 3 – 4.6 $V_{Li}$ at a ~C/10 rate with a 1 h hold in cycle 1 and a ~C/5 rate with a 1 h hold in cycle two. The carrier gas was Ar.*

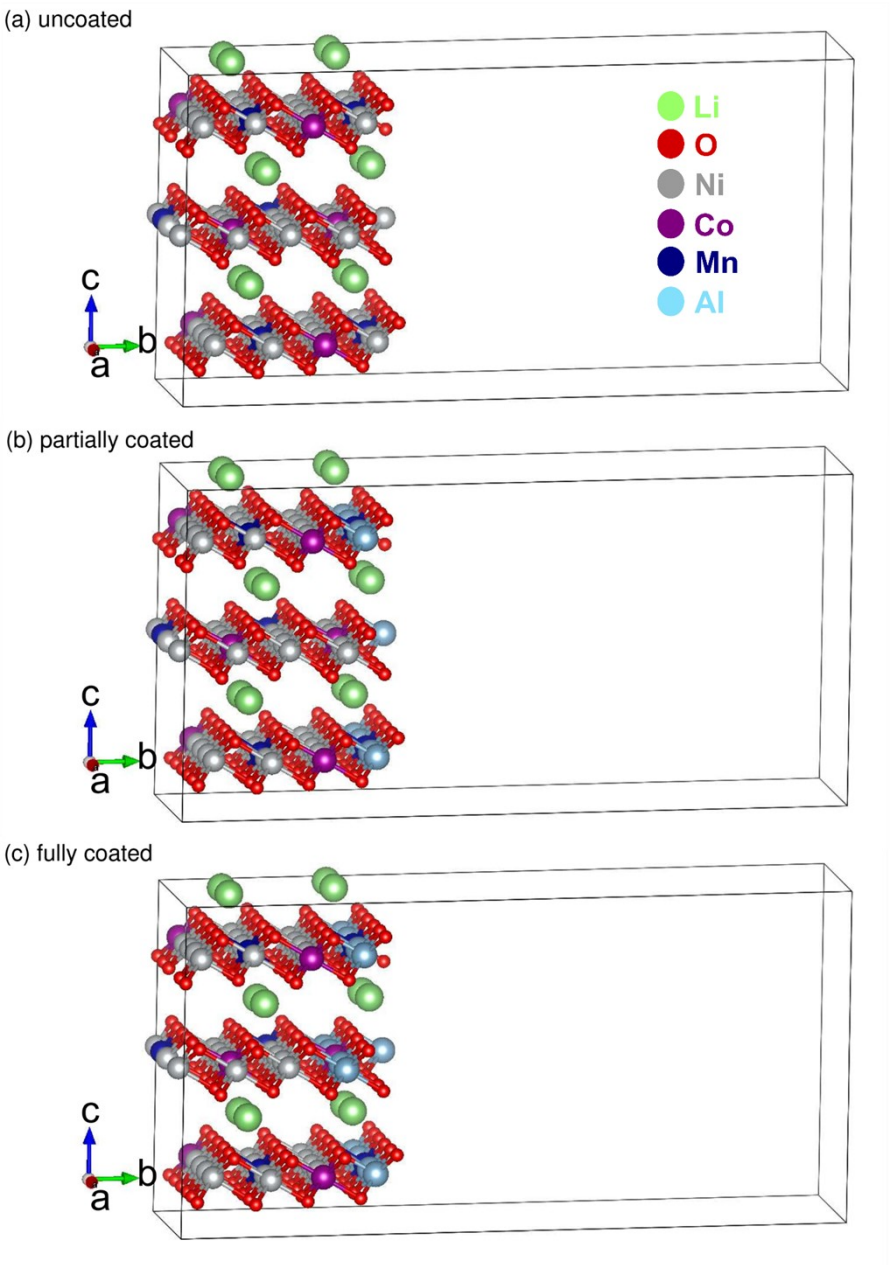


*Figure S21: Supercell (5 x 4 x 1) of the rhombohedral LNO unit cell where each layer has 2 Ni ion replaced by Mn and 2 by Co, with all dopant atoms surrounded only by Ni atoms. Oxygen is in red, Lithium is in green, Nickel is in grey, Co is in purple, Mn is dark blue and Aluminium is light blue. 75 % of the Li were removed from the structure to achieve an experimentally relevant state of delithiation. Three different structures (uncoated in (a), partially coated in (b) and fully coated in (c)) were created, each with a vacuum of ~20 Å along the b direction to mimic the effect of a coated/uncoated surface.*

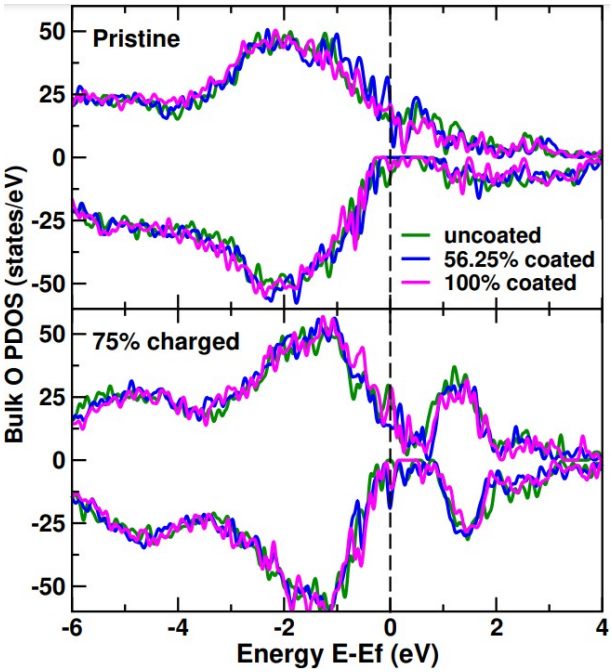


*Figure S22: Electronic density of states for the Ni, Mn, Co and O averaged across the NMC811 supercell with either no Al present (green), Al partially (56.25 %) substituting the surface transition metals (blue) or fully substituting the surface transition metals (magenta). A vacuum (extending away by 20 Å) is applied to the surface and the structure allowed to equilibrate at 0 K after 75 % Li was removed from the structure.*

No significant difference in the average O *p* orbital populations (dominated by O in the bulk) are observed between the uncoated, partially coated and fully coated NMC811 supercells after 75 % of the Li was removed (**Figure S21**). This indicates that the presence of Al on the surface does not influence the hybridised Ni *d* – O *p* bond in the bulk. Therefore, during delithiation of the NMC811, the bulk oxygen can still participate in redox.

*Table S14: Discharge capacities of representative cells for the NMC811 | LP57+2 wt% VC | Graphite before and after ageing with the subsequent discharge capacity of the diagnostic aged NMC811 | LP57 | Li cell. These cycles were all charged at C/20, assuming a practical capacity of 200 mAhg$^{-1}$.*

| **Sample** | **Discharge capacities / mAhg$^{-1}$** | | |
|---|---|---|---|
| | *Cycle 1 (vs. graphite)* | *Cycle 1042 (vs. graphite)* | *Diagnostic (vs. Li)* |
| **NMC811** | 193 | 94 | 99 |
| **ALD NMC811** | 168 | 101 | 120 |

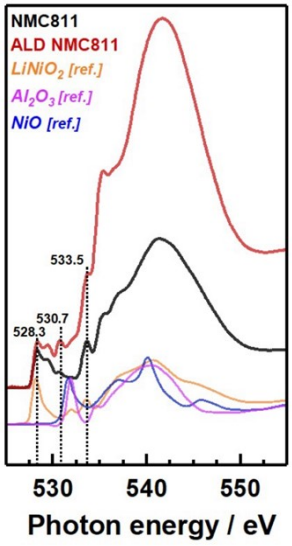


*Figure S23: O K-edge spectra of the uncycled NMC811 (black) and ALD NMC811 (red) electrodes are presented with spectra from reference samples of $LiNiO_2$ (orange), $\gamma$-$Al_2O_3$ (magenta) and NiO (blue). The first dashed line at 528.3 eV is assigned to O in NMC811, while the peaks at 530.7 and 533.5 eV are assigned to molecular oxygen[20] and $Li_2CO_3$ impurities on the electrode surface, respectively.*

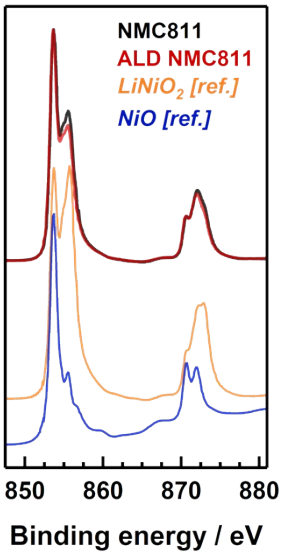


*Figure S24: Ni L-edge spectra of the uncycled NMC811 (black) and ALD NMC811 (red) electrodes are presented along with spectra from reference samples of $LiNiO_2$ (orange) and NiO (blue).*

*Table S15 Ratios of the high energy (855.8 eV) and low energy (853.7eV) components within the $L_3$ peak of the Ni L-edge XAS spectrum for the uncoated NMC811 and the ALD NMC811 electrodes at different states. The aged electrodes were from NMC811 | graphite cells using the LP57 + 2 wt% VC electrolyte.*

| | **855.8 eV: 853.7 eV ratio in $L_3$ Casted electrode** | **855.8 eV: 853.7 eV ratio in $L_3$ Cycle 1, 4.4 $V_{Li}$** | **855.8 eV: 853.7 eV ratio in $L_3$ Diagnostic, 4.4 $V_{Li}$** |
|---|---|---|---|
| **NMC811** | 2.05 | 2.75 | 1.62 |
| **ALD NMC811** | 1.90 | 2.96 | 2.40 |

*Table S16: Summary of the species identified in $^{1}H$ solution NMR spectra after cycling NMC|LFP coin cells with electrolyte and its component solvents.*

| **Solvent & Test Potential** / *vs* $V_{Li+}$ | **Nucleus** | **δ** / ppm | **Species** |
|---|---|---|---|
| EC/EMC (3/7) | $^{1}H$ | 4.49 (s)<br>4.11 (q) | Ethylene carbonate (EC) |
| | $^{1}H$ | 3.68 (s)<br>1.20 (t) | Ethyl methyl carbonate (EMC) |
| | $^{1}H$ | 3.39 (s) | Water |
| | $^{1}H$ | 10.52 (d, $^{1}J_{F-H}$ = 414 Hz) | HF depending on different coordinations and complexes[21] |
| EC/EMC (3/7) (4.6 V) | $^{1}H$ | 8.25 (s)<br>8.19 (s) | Lithium formate<br>Formic acid |
| | $^{1}H$ | 7.77 (s) | Vinylene carbonate (VC) |
| | $^{1}H$ | 6.62 (dd, $^{3}J_{H-H}$ = 5.6, 1.9 Hz)<br>4.75 (difficult to deconvolute)<br>3.81 (s) | Methoxyethylene carbonate (MEC) |
| | $^{1}H$ | 6.57 (ddd, $^{2}J_{F-H}$ = 64.5 Hz, $^{3}J_{H-H}$ = 4.1, 0.8 Hz)<br>4.76 (difficult to deconvolute)<br>4.68 (difficult to deconvolute) | Fluoroethylene carbonate (FEC) |
| | $^{1}H$ | 6.34 (q, $^{3}J_{F-H}$ = 57.4 Hz, $^{2}J_{H-H}$ = 5.0 Hz)<br>3.78 (s)<br>1.49 (dd, $^{2}J_{F-H}$ = 21.4 Hz, $^{3}J_{H-H}$ = 5.0 Hz | 1-Fluorinated ethyl methyl carbonate (FEMC) |
| | $^{1}H$ | 5.80 (s)<br>4.21 (s) | Methanediol |
| | $^{1}H$ | 5.69 (s)<br>4.20 (s)<br>3.57 (s) | Methyoxymethanol |
| | $^{1}H$ | 3.52 (singlet observed)<br>1.04 (singlet observed) | Ethanol/Lithium ethoxide |
| | $^{1}H$ | 3.33 (s) | Lithium methoxide |
| | $^{1}H$ | 4.10 (q, obscured by EMC)<br>3.17 (d, $^{3}J_{H-H}$ = 5.3 Hz) | Methanol |

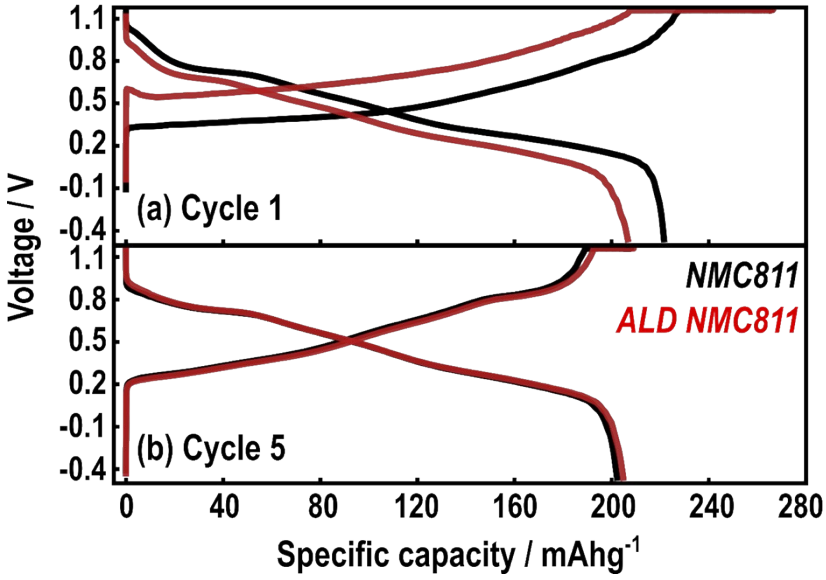


*Figure S25: Voltage profiles of (a) NMC811 | delithiated LFP after one cycle, and (b) after five cycles using a 1 M $LiPF_6$ in EC/EMC (3/7 (v/v)) electrolyte. Cells are cycled at a C/10 rate (assuming a practical capacity of 200 $mAhg^{-1}$) between -0.46 – 1.16 V (22 °C) with a 60 h hold at the top of charge. The NMC811 with no coating is in black whilst the ALD NMC811 is in red. After the cycling, the cell is disassembled and the separator extracted for solution NMR analysis.*

As seen in other electrochemical cycling data, the initial lower capacity obtained from the ALD NMC811 is offset by the improved capacity retention compared to the uncoated NMC811.

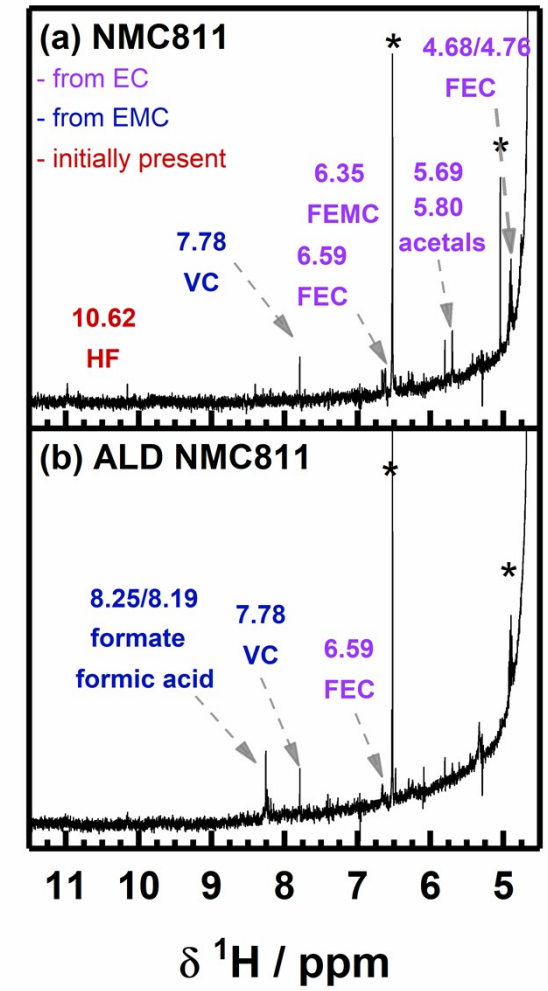


*Figure S26: Normalised $^{1}H$ solution NMR spectra of the EC/EMC electrolyte extracted from the glass fibre separator after cycling (a) NMC811 | delithiated LFP, and (b) ALD NMC811 | delithiated LFP coin cells. Coin cells were cycled between -0.46 – 1.16 V (equivalent to 3.0 – 4.6 $V_{Li}$) for **1 cycle** with a 60 h hold at the top of charge. Assignments in purple indicate species derived from EC, assignments in blue are derived from EMC, and red indicates electrolyte species initially present. DMSO-$d_6$ was used as a solvent in all cases. $^{1}H$ spectra are normalised to the EMC peak intensities. Asterisks (*) mark the impurities from the DMSO solvent.*

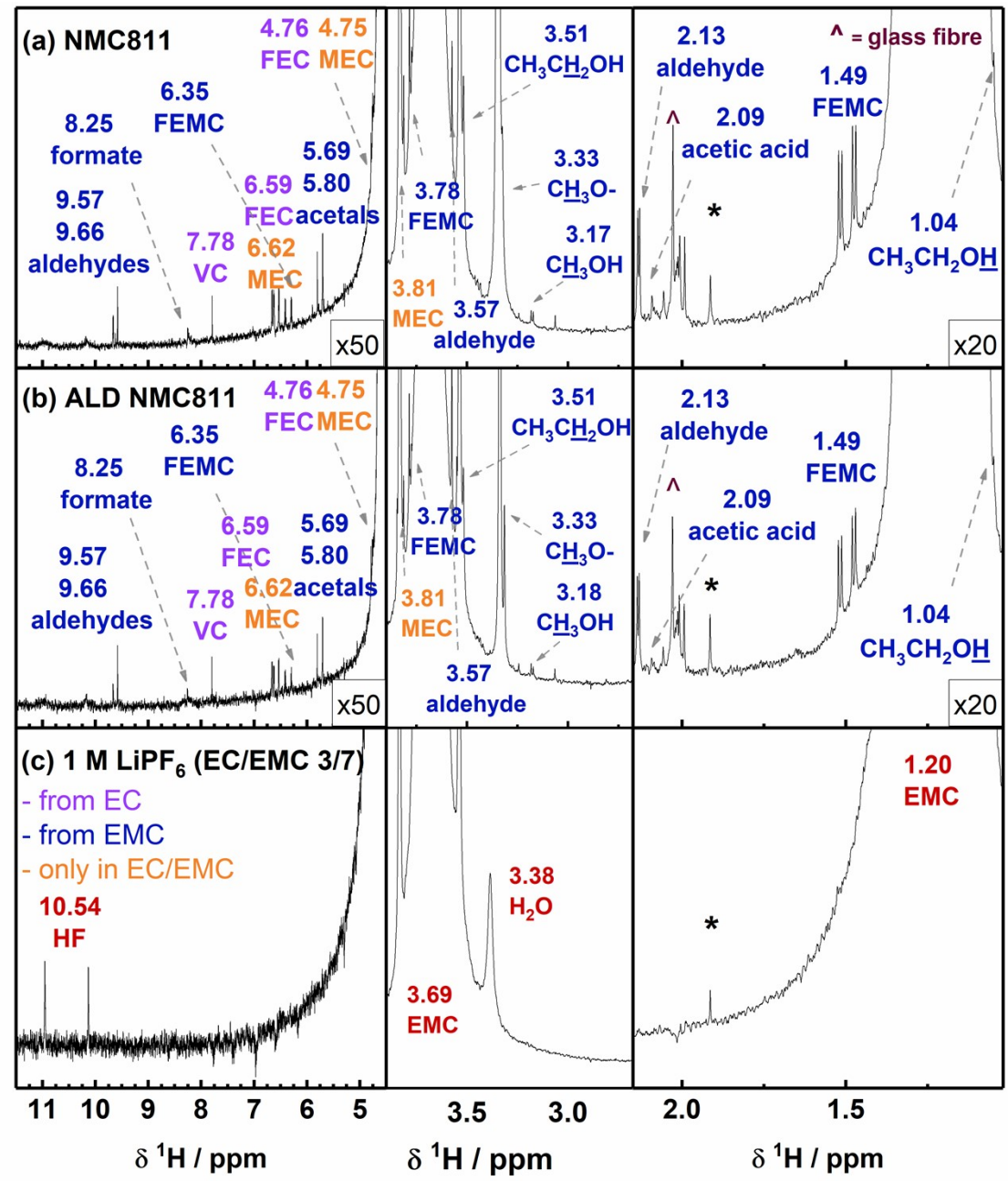


*Figure S27: Normalised $^{1}H$ solution NMR spectra of the EC/EMC electrolyte extracted from the glass fibre separator after cycling (a) NMC811 | delithiated LFP, (b) ALD NMC811 | delithiated LFP coin cells, and (c) the as mixed 1 M $LiPF_6$ in EC/EMC (3/7) after resting for 24 h. Coin cells were cycled between -0.46 – 1.16 V (equivalent to 3.0 – 4.6 $V_{Li}$) for **5 cycles** with 60 h holds at the top of charge. Assignments in purple indicate species derived from EC, assignments in blue are derived from EMC, and red indicates electrolyte species initially present. DMSO-$d_6$ was used as a solvent in all cases. $^{1}H$ spectra are normalised to the EMC peak intensities. Asterisks (*) mark the impurities from the DMSO solvent and the arrow (^) indicates the glass fibre products.*

## ESI 7: Multi-site complexation (MUSIC) model

A model based on partial charges, entitled the multi-site complexation (MUSIC) model predicts the affinity of a proton to bond to oxygen based on the expected electrostatic repulsion from nearby cation centres.[22,23] At this bridging O, the net electric charge relative to the Pauling bond valence ($\sigma$) of the O is the sum of the partial charges contributed by each bonded cation

($+\frac{3}{5}$ for an Al(V) site).[24] The bridging oxygen has a bond valence $\sigma$ = -0.8 whilst the terminal O in the Al-OH group is less basic at $\sigma$ = -0.4 (due to an additional +1 charge from the bonded hydroxyl proton). Deviations to the Pauling bond valence due to factors like hydrogen bonding to the target O site and non-symmetric distribution of charge along the Al-O bonds due to different bond lengths were not considered in this simplified analysis.[22,23] Presumably other permutations of Al(IV), Al(V) and Al(VI) sites (*e.g.* amongst the 5 cases proposed by Peri)[25] that enable both the chemisorption of water and an increase in coordination number for the Al site also exist. Use of this model highlights the role of Lewis acid (undercoordinated Al) and basic (appropriate O) sites in forming environments for which protons can favourable bond and thereby enabling such scavenging reactions. Chemical characteristics of the $Al_2O_3$ coating such as having undercoordinated Al environments are therefore implied to be a desirable feature in tuning the coating's ability to sequester water from the Li-ion battery electrolyte.

## References:


1 H. D. Morris and P. D. Ellis, *J. Am. Chem. Soc*, 1989, **111**, 6045–6049.
2 D. Muller, W. Gessner, H.-J. Behrens and G. Scheler, *Chemical Physical Letters*, 1981, **79**, 59–62.
3 E. Witt, S. Nakhal, C. V. Chandran, M. Lerch and P. Heitjans, *Zeitschrift fur Physikalische Chemie*, 2015, **229**, 1327–1339.
4 V. Lacassagne, C. Bessada, P. Florian, S. Bouvet, B. Ollivier, J. P. Coutures and D. Massiot, *Journal of Physical Chemistry B*, 2002, **106**, 1862–1868.
5 P. J. Chupas, D. R. Corbin, V. N. M. Rao, J. C. Hanson and C. P. Grey, *Journal of Physical Chemistry B*, 2003, **107**, 8327–8336.
6 C. V. Chandran, C. E. A. Kirschhock, S. Radhakrishnan, F. Taulelle, J. A. Martens and E. Breynaert, *Chemical Society Reviews*, 2019, **48**, 134–156.
7 M. Dressler, M. Nofz, F. Malz, J. Pauli, C. Jäger, S. Reinsch and G. Scholz, *Journal of Solid State Chemistry*, 2007, **180**, 2409–2419.
8 L. B. Alemany and G. W. Kirker, *Journal of American Chemical Society*, 1986, **108**, 6158–6162.
9 S. K. Lee, S. Y. Park, Y. S. Yi and J. Moon, *Journal of Physical Chemistry C*, 2010, **114**, 13890–13894.
10 E. Lippmaa, A. Samoson and M. Mági, *Journal of American Chemical Society*, 1986, **108**, 1730–1735.
11 J. B. d'Espinose de Lacaillerie, C. Fretigny and D. Massiot, *Journal of Magnetic Resonance*, 2008, **192**, 244–251.
12 N. M. Trease, I. D. Seymour, M. D. Radin, H. Liu, H. Liu, S. Hy, N. Chernova, P. Parikh, A. Devaraj, K. M. Wiaderek, P. J. Chupas, K. W. Chapman, M. S. Whittingham, Y. S. Meng, A. Van Der Van and C. P. Grey, *Chemistry of Materials*, 2016, **28**, 8170–8180.
13 C. Delmas, D. Carlier, G. Ceder, M. Ménétrier and C. P. Grey, *Physical Review B - Condensed Matter and Materials Physics*, 2003, **67**, 1–14.
14 D. Iuga, H. Schäfer, R. Verhagen and A. P. M. Kentgens, *Journal of Magnetic Resonance*, 2000, **147**, 192–209.
15 H. E. Gottlieb, V. Kotlyar and A. Nudelman, *Journal of Organic Chemistry*, 1997, **62**, 7512–7515.
16 M. Leskes, A. J. Moore, G. R. Goward and C. P. Grey, *Journal of Physical Chemistry C*, 2013, **117**, 26929–26939.

17 J. Borau-Garcia, D. V. Gutsulyak, R. J. Burford and W. E. Piers, *Dalton Transactions*, 2015, **44**, 12082–12085.
18 D. R. Neuville, L. Cormier and D. Massiot, *Geochimica et Cosmochimica Acta*, 2004, **68**, 5071–5079.
19 D. Massiot, F. Fayon, M. Capron, I. King, S. Le Calvé, B. Alonso, J. O. Durand, B. Bujoli, Z. Gan and G. Hoatson, *Magnetic Resonance in Chemistry*, 2002, **40**, 70–76.
20 C. Århammar, A. Pietzsch, N. Bock, E. Holmström, C.M. Araujo, J. Gråsjö, S. Zhao, S. Green, T. Peery, F. Hennies, S. Amerioun, A. Föhlisch, J. Schlappa, T. Schmitt, V.N. Strocov, G.A. Niklasson, D.C. Wallace, J. Rubensson, B. Johansson and R. Ahuja, *Proc. Natl. Acad. Sci. U.S.A.*, 2011, **108**, 6355-6360,
21 B. L. D. Rinkel, D. S. Hall, I. Temprano and C. P. Grey, *Journal of the American Chemical Society*, 2020, **142**, 15058–15074.
22 T. Hiemstra, P. Venema and W. H. Van Riemsdijk, *Journal of Colloid and Interface Science*, 1996, **184**, 680–692.
23 P. Venema, T. Hiemstra, P. G. Weidler and W. H. Van Riemsdijk, *Journal of Colloid and Interface Science*, 1998, **198**, 282–295.
24 L. Pauling, *Journal of the American Chemical Society*, 1929, **51**, 1010–1027.
25 J. B. Peri, *The Journal of Physical Chemistry*, 1965, **69**, 220–230.